Generalized theory for the dynamic analysis of thin shells with application to circular cylindrical geometries

by

Raydin Salahifar [a] , Magdi Mohareb [b]

[a] Baha'i Institute for Higher Education, Tehran, Iran, Tel.: +989125472292, Raydin.Salahifar@bihe.org, RaydinSalahifar@yahoo.com (Corresponding author)

[b] Department of Civil Engineering, University of Ottawa, Ottawa, ON, Canada K1N 6N5, MMohareb@uottawa.ca

Abstract

A generalized theory is formulated for the analysis of thin shells of general curvatures based on the variational form of the Hamiltonian functional in conjunction with tensor calculus. Simplifying approximations and subtle inconsistencies made at the early stages of common classical formulations are avoided herein, and hence, the present treatment leads to field equations and boundary conditions that are accurate and consistent. The theory is then specialized to circular cylindrical shells. The well -known field equations of Flugge and Donnell-Mushtari-Vlasov (DMV) theories are recovered as consistent approximations from the present theory. Closed form solutions are then developed for the present and past cylindrical shell theories by Flugge, Timoshenko, and DMV. A comparative study is conducted to assess and quantify the effects of approximations made in classical theories on the predicted displacements and stresses.

Keywords

Thin shell theory, shells with general curvature, cylindrical shells, Hamilton principle, steady state response, Tensor-based formulation

This article is to be cited as
Salahifar R, Mohareb M, (2019) Generalized theory for the dynamic analysis of thin shells with application to circular cylindrical geometries, Thin-Walled Structures, 139: 347-36.

The copy-edited version of this article is available at: https://doi.org/10.1016/j.tws.2018.11.021.

1. Introduction

Thin shells are commonly encountered in structural applications, onshore and offshore pipelines, and mechanical equipment, where they are commonly subjected to a variety of static, quasi-static or dynamic loading. Under such conditions, shells may undergo a complex deformational behaviour. The literature reveals the presence of several seemingly conflicting stress-deformation theories for thin-shells. The selection for a proper shell theory in a given application requires (a) an in-depth understanding of the underlying assumptions, and (b) a critical assessment of various assumptions on the predictive ability of the theory. Within this context, the present study contributes to both objectives by developing a theory for thin shells of general geometries while keeping the assumptions and simplifications made to a minimum. The formulation is then specialized to circular cylindrical shells. By applying various approximations to the resulting formulation, other well-established cylindrical thin-walled shell theories are recovered as special cases.

1.1 Literature Review

Classical linear shell theories involve the work of Timoshenko [1], Novozhilov [2], Koiter [3], Flugge [4] (and [5]), Saada [6], DMV [7] and Niordson [7]. Non-linear shell theories include the work of Leonard [8], Sanders [9], Koiter [10] , [11] and Budiansky [12]. The comprehensive monograph by Leissa [13] provides a detailed report on the wide range of shell theories available. Libai and Bert [14] developed mixed variational principles for the elastic small-strains and large-rotation analysis of shells based on the Kirchhoff-Love hypothesis. Muneeb et al. [15] developed a higher order theory for the dynamic response of isotropic thermo-elastic analysis of cylindrical shells. Kolesnikov [16] formulated a refined theory for the vibration of multilayer orthotropic cylindrical shells through a series expansion of the radial displacement field in terms of the shell thickness. Through asymptotic expansion of the general equilibrium equations for a general state of stress in three-dimensional bodies, Niordson [17] formulated a two-dimensional shell theory for circular cylindrical shells. Ugrimov [18] presented a layerwise generalized theory for the elasto-dynamic analysis of multilayer plates by expanding the displacement components of each layer as power series of the transverse coordinate. Ciarlet and Gratie [19] developed an approach to minimize the quadratic problem arising in Koiter's linear shell theory. Using the Cosserat surface model, Birsan [20] presented a theory for porous elastic shells by employing the Nunziato-Cowin

theory of elastic materials with voids, to characterize the porosity within the shell. Altenbach et al. [21] developed a linear shell theory that accounts for transverse shear and surface stresses. Weicker et al. ([22] and [23]) developed a closed form solution for the static analysis of thin-walled pipes [22], and a finite element formulation [23]. Salahifar and Mohareb [24] formulated a closed form solution for circular cylindrical shells under harmonic forces. Amabili and Reddy [25] derived a consistent higher-order shear deformable theory for doubly curved shells of general geometries based on non-linear strain-displacement expressions. Their solution accounts for geometric imperfections. Paimushin [26] developed a large displacement shell theory based on the classical Kirchhoff-Love assumption. The solution accounts for deformations in the transverse direction by introducing additional displacement fields. Salahifar and Mohareb [27] formulated a finite element for the analysis of circular cylindrical thin shells under harmonic forces based on shape functions that satisfy the governing field equations. Favata and Podio-Guidugli [28] developed a theory of linearly elastic orthotropic shells with potential application to the continuous modeling of carbon nanotubes. Sansour et al. [29] developed a computationally efficiently strain gradient formulation that captures the scale effects of shell-like structures when one of the dimensions is very small relative to the other two dimensions. Xuea et al. [30] extended the Karman-Donnell theory for shallow cylindrical shells to account for large deformations. Based on an expansion of the axisymmetric equations of elasticity, Zozulya [31] developed a high-order theory for functionally graded axisymmetric cylindrical shells using Legendre polynomial series. Carrera et al. [32] (and [33]) developed a unified hierarchical formulation for multilayered composite structures, which enables the implementation of multiple plate/shell theories and finite elements based on a few fundamental nuclei. Cattabiani et al. [34] developed a variational shell theory that approximates the solution for the vibration problem as a sum of shape functions that identically satisfy the equilibrium equations while satisfying the weak form of the boundary conditions. Chowdhurya et al. [35] developed a state-based peridynamic formulation for the linear elastic analysis of shells that captures discontinuities by expressing the equations of motion in integro-differential form as opposed to partial differential equations. Zveryayev [36] developed an itertative shell solution, in which the three-dimensional equations of the elasticity in curvilinear coordinates were reduced using the Saint-Venant semi-inverse method. Awrejcewicz et al. [37] presented a mathematical model for nonlinear analysis of micro-shells that accounts for temperature-deformation coupling. Using Hamilton's principle, Wangab et al. [38] developed a first-order shear deformable shell

theory for the free and transient vibration analysis of composite laminated cylindrical shells by partitioning the radial displacement field into bending and shear components. Okhovat and Bostrom [39] derived a hierarchy of shell equations in the form of power series in terms of the shell thickness for the dynamic analysis of orthotropic cylindrical shells. Qingshan et al. [40] developed a first-order shear deformable shell theory for the free and transient vibration analysis of laminated open cylindrical shells with general boundary conditions.

1.2 Common Assumptions

In general, the theory of thin shells involves two aspects: a) developing the governing field equations and the boundary conditions and b) providing solutions to the field equations for problems with specific geometries, boundary conditions, and loading. Most thin-shell formulations are based on the following assumptions:

1. Conservation of normals: All points lying on a normal to the middle surface before deformation remain on the normal to the deformed middle surface. This implies a linear distribution of the in-plane displacements across the thickness of the shell and zero shear strains in the planes normal to the mid-surface.

2. A surface at a distance z from the middle surface before deformation will remain at the same distance from the middle surface after deformation, and

3. Displacements are small compared to the radii of curvature of the middle surface. This signifies that the curvatures of the shell mid-surface after deformation are considered nearly equal to the curvatures before deformation.

1.3 Differences among Shell Theories

A survey of the literature reveals the presence of multiple cylindrical thin-shell theories. The differences between these shell theories are attributed to the following aspects:

1. The adoption of different strain-displacement relationships: In some theories (e.g., Timoshenko[1] and Flugge [3]) the strain-displacement relationships are obtained based on geometric inspection of an infinitesimal portion of the shell undergoing deformation. In other theories (e.g., Novozhilov [2], Saada [6] and Niordson [7]), a vector or tensor analysis approach is adopted.

2. The use of different methodologies in formulating the governing equations: In most theories (e.g., Timoshenko [1], Flugge [4], Saada [6] and Niordson [7]), equilibrium equations are obtained based on the force equilibrium of an infinitesimal shell element, while others (e.g., Novozhilov [2]) adopt a variational approach.

3. The enforcement of additional simplifications: Most researchers have applied various simplifications at different stages of the formulation, which had implications on the final form of the governing field equations and the boundary conditions. For example, Novozhilov [2] has neglected some of the terms in the expression of total potential energy compared to the other terms.

4. Inconsistencies in enforcing simplifications: Most theories (Timoshenko [1], Saada [6], Niordson [7], etc.) involved slight inconsistencies in their simplifications. For example, the effect of the shell thickness in the strain expression is neglected in some terms, but kept in other terms within the same formulation. These types of inconsistencies, in most cases, arose from separating the membrane strains from the bending strains.

Given the above discrepancies, it is difficult to judge which theories provide superior results and which are most suited for a given engineering problem. While, in some cases, there could be some qualitative notion on which theory could be judged to provide reliable predictions of the response, a systematic quantitative comparative assessment is missing. For a given problem, it becomes difficult to judge how much error is attributed to treating a given problem as a thin shell and how much is attributed to the approximations and treatments specific to the adopted theory. In order to elucidate the problem, the present treatment focuses on developing a generalized thin shell theory in which the strain-displacement relationships are thoroughly formulated based on tensor calculus in conjunction with assumptions that are well accepted within the framework of all thin-shell theories, while avoiding inconsistencies.

2. Generalized Thin Shell Theory Formulation

2.1 Geometric preliminaries

In general, a thin shell can be considered as a group of parallel curved surfaces in the immediate vicinity of the middle surface. Point P_0 on a surface can be defined by two curvilinear coordinates of a two dimensional subspace ($\mathbf{R}^{\alpha}$) of the general three-dimensional

space ($\mathbf{R}^i$). As a notation convention, all Latin indices take the values 1, 2, 3, while Greek indices take the values 1 and 2. This implies that, in a curvilinear coordinate system x^i, the geometry of any of those surfaces can be defined by two curvilinear coordinates x^α within the middle surface and an additional coordinate x^3 normal to the middle surface (Figure 1). In a Cartesian coordinate system χ^i with $\mathbf{I}_i$ as a covariant unit vector, position vector $\mathbf{R}\left(\chi^i_{P_1}(t)\right) = \chi^i_{P_1}(t)\mathbf{I}_i$ at time t for a point P_1 within the shell (Figure 1), can be defined as the vector sum of position vector $\mathbf{r}\left(\chi^i_{P_0}(t)\right) = \chi^i_{P_0}(t)\mathbf{I}_i$ of its projection P_0 on the middle surface and vector $\vec{P_0P_1}$, i.e.,

$$\mathbf{R}\left(\chi^i_{P_1}(t)\right) = \mathbf{r}\left(\chi^i_{P_0}(t)\right) + \vec{P_0P_1}\left(\chi^i_{P_0}(t), \chi^i_{P_1}(t)\right) \tag{1}$$

In Eq. 1, expressing the Cartesian coordinates χ^i for points P_0 and P_1 (i. e. $\chi^i_{P_0}(t)$ and $\chi^i_{P_1}(t)$) in terms of curvilinear coordinates x^i enables expressing the position vectors for points P_0 and P_1 as $\mathbf{r}\left(\chi^i_{P_0}(t)\right) = \chi^i\left(x^j_{P_0}, t\right)\mathbf{I}_i$ and $\mathbf{R}\left(\chi^i_{P_1}(t)\right) = \chi^i\left(x^j_{P_1}, t\right)\mathbf{I}_i$, respectively. Thus, Cartesian coordinates χ^i appearing in Eq. 1 can be expressed in terms of curvilinear coordinates x^i yielding

$$\mathbf{R}\left(\chi^i\left(x^j_{P_1}, t\right)\right) = \mathbf{r}\left(\chi^i\left(x^j_{P_0}, t\right)\right) + \vec{P_0P_1}\left(\chi^i\left(x^j_{P_0}, t\right), \chi^i\left(x^j_{P_1}, t\right)\right) \tag{2}$$

or

$$\mathbf{R}\left(\chi^i\left(x^j_{P_1}, t\right)\right) = \mathbf{r}\left(\chi^i\left(x^\alpha_{P_0}, t\right)\right) + x^3\mathbf{a}_3 \tag{3}$$

in which unit vector $\mathbf{a}^3 = \left(\mathbf{a}_1 \otimes \mathbf{a}_2\right) / \left|\mathbf{a}_1 \otimes \mathbf{a}_2\right|$ is normal to the plane defined by base vectors $\mathbf{a}_\alpha = \partial\mathbf{r} / \partial x^\alpha$. Equation 3 provides the transformation of a shell surface from curvilinear coordinate system x^i into Cartesian coordinate system χ^i. It can be re-written as

$$\mathbf{R}\left(x^1, x^2, x^3, t\right) = \mathbf{r}\left(x^1, x^2, t\right) + x^3\mathbf{a}_3 \tag{4}$$

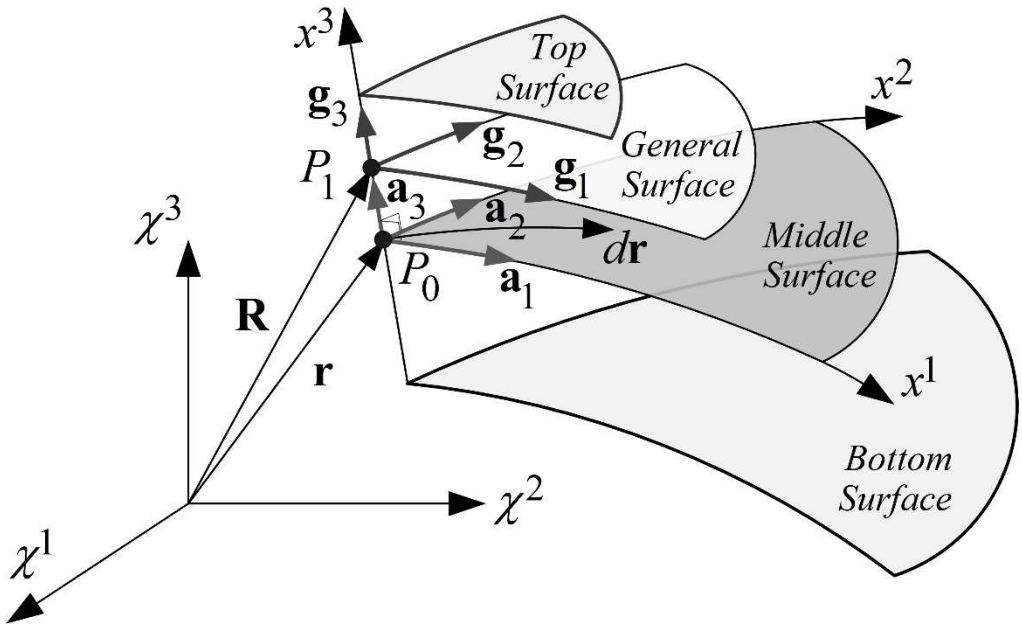

Figure 1 - Shell Geometry

In a similar manner, bases $\mathbf{g}_i = \partial\mathbf{R}/\partial x^i$ pertain to a general surface within the shell volume. It can be shown that base vectors $\mathbf{g}_\alpha$ on a surface parallel to the mid-surface are related to the base vectors of the middle surface $\mathbf{a}_\gamma$ through $\mathbf{g}_\alpha = \mu_\alpha^\gamma \mathbf{a}_\gamma$. Here, $\mu_\alpha^\gamma = \delta_\alpha^\gamma - x^3 \bar{b}_\alpha^\gamma$ is the shifter tensor, δ_α^γ is the Kronecker delta tensor and $\bar{b}_\alpha^\gamma$ is the mixed curvature tensor for the middle surface, which is related to the Christoffel symbol through $\bar{b}_\alpha^\gamma = -\bar{\Gamma}_{3\alpha}^\gamma$. Christoffel symbols of the second kind are defined as $\Gamma_{ij}^k = g^{kl}\left(g_{li,j} + g_{lj,i} - g_{ij,l}\right)/2$ and, as a matter of convention, all symbols with a bar denote quantities pertaining to the middle surface, unless mentioned otherwise.

In general, the contravariant counterparts of the covariant base vectors are $\mathbf{g}^\alpha = \lambda_\gamma^\alpha \mathbf{a}^\gamma$ and $\mathbf{g}^3 = \mathbf{a}^3$, in which $\lambda_\gamma^\alpha \mu_\beta^\gamma = \delta_\beta^\alpha$ and the covariant and contravariant base vectors are related through $\mathbf{g}_j \cdot \mathbf{g}^i = \delta_j^i$. The covariant and contravariant metric tensors for surfaces parallel to the middle surface are respectively expressed as

$$g_{\alpha\beta} = \mathbf{g}_\alpha \cdot \mathbf{g}_\beta = \mu_\alpha^\gamma \mu_\beta^\delta a_{\gamma\delta} \quad , \quad g^{\alpha\beta} = \mathbf{g}^\alpha \cdot \mathbf{g}^\beta = \lambda_\gamma^\alpha \lambda_\delta^\beta a^{\gamma\delta} \tag{5a-b}$$

where $a_{\gamma\delta}$ and $a^{\gamma\delta}$ are the covariant and contravariant metric tensors of the middle surface, respectively, and defined as

$$a_{\gamma\delta} = \mathbf{a}_\gamma \cdot \mathbf{a}_\delta \quad , \quad a^{\gamma\delta} = \mathbf{a}^\gamma \cdot \mathbf{a}^\delta \tag{6a-b}$$

The second fundamental tensor of the surface (curvature tensor) is defined as $\bar{b}_{\alpha\beta} = \mathbf{a}_{3,\alpha} \cdot \mathbf{a}_\beta$. The Jacobian g at a generic point within the shell, given by $g = \det\left(g_{ij}\right)$, represents a differential element of volume.

2.2 **Strains in Thin Shells**

Using the Lagrangian approach, the strain tensor is defined in terms of the metric tensor through $\eta_{ij} = \left(\hat{g}_{ij} - g_{ij}\right)/2$. One can show [41] that the strain-displacement relationship is defined by $\eta_{ij} = \frac{1}{2}\left(U_i \,|_j + U_j \,|_i + U^k \,|_i \, U_k \,|_j\right)$ in which, the notation $|_i$ denotes the covariant derivative of the argument vector with respect to $i = 1,2,3$. Under the small deformation assumption, the nonlinear terms $U^k \,|_i \, U_k \,|_j$ are negligible compared to the linear terms. Also, for thin shells, the strains can be resolved into in-plane components $\eta_{\alpha\beta}$ and out-of-plane components $\eta_{\alpha 3} = \eta_{3\alpha}$ and η_{33}, and the displacement strain relations can be approximated by:

$$\eta_{\alpha\beta} = \tfrac{1}{2}\left(U_\alpha \,|_\beta + U_\beta \,|_\alpha\right) \;,\; \eta_{\alpha 3} = \eta_{3\alpha} = \tfrac{1}{2}\left(U_\alpha \,|_3 + U_3 \,|_\alpha\right) \;,\; \eta_{33} = \tfrac{1}{2}\left(U_3 \,|_3 + U_3 \,|_3\right) \tag{7a-c}$$

According to Assumption 2 in Section 1.2 , the strain normal to the mid-surface vanishes, i.e. $\eta_{33} = \frac{1}{2}\left(U_3 \,|_3 + U_3 \,|_3\right) \simeq 0$. Also, according to Assumption 1 in Section 1.2 , the transverse shear strains acting on the planes perpendicular to the mid-surface are negligible for thin shells leading to the simplification $\eta_{\alpha 3} = \eta_{3\alpha} \simeq 0$.

2.3 **Displacements of a Point within the Shell**

In general, displacement vector $\mathbf{U}$ of a point A offset from the middle surface can be defined as

$$\mathbf{U} = U_i\left(x^1, x^2, x^3, t\right)\mathbf{g}^i = U^i\left(x^1, x^2, x^3, t\right)\mathbf{g}_i \tag{8}$$

where U_i and U^i are, respectively, the covariant and contravariant components of the displacement vector in the x^i coordinate system. Displacement vector $\mathbf{U}$ is related to position vector $\mathbf{R}$ in the undeformed configuration (Figure 2) and position vector $\hat{\mathbf{R}}$ in the deformed configuration through $\mathbf{U} = \hat{\mathbf{R}} - \mathbf{R}$. Vectors $\mathbf{R}$ and $\hat{\mathbf{R}}$ at point A are related to vectors $\mathbf{r}$ and $\hat{\mathbf{r}}$ at the corresponding point B on the mid-surface and unit vectors normal to the mid-surface $\mathbf{a}_3$ and $\hat{\mathbf{a}}_3$ as

$$\mathbf{U} = \hat{\mathbf{R}} - \mathbf{R} = \left(\hat{\mathbf{r}} + \hat{x}^3\hat{\mathbf{a}}_3\right) - \left(\mathbf{r} + x^3\mathbf{a}_3\right) = \left(\hat{\mathbf{r}} - \mathbf{r}\right) + x^3\left(\hat{\mathbf{a}}_3 - \mathbf{a}_3\right) \tag{9}$$

Noting that the difference $\mathbf{u} = \hat{\mathbf{r}} - \mathbf{r}$ is the displacement vector at point B and $\mathbf{a}_3$, $\hat{\mathbf{a}}_3$ are the unit vectors normal to the mid-surface at point B before and after deformation, the difference $\boldsymbol{\theta} = \hat{\mathbf{a}}_3 - \mathbf{a}_3$ characterizes the angle of rotation of the middle surface and thus Eq. 9 can be re-written as

$$\mathbf{U} = \mathbf{u}\left(x^1, x^2, t\right) + x^3\boldsymbol{\theta}\left(x^1, x^2, t\right) \tag{10}$$

Assumption 1 in Section 1.2, regarding the normality to the mid-surface, implies zero shear strains on the planes perpendicular to the mid-surface, i.e. $\eta_{3\alpha} = \eta_{\alpha 3} = \left(U_\alpha|_3 + U_3|_\alpha\right)/2 = 0$. It can be used [41] to relate the displacement $\mathbf{U}$ of arbitrary point A, located at a distance $x^3 \neq 0$ from the shell mid-surface within the shell, to those of its projection on the middle surface, point B ($\mathbf{u} = u_i\mathbf{a}^i$), through

$$\mathbf{U} = U_\alpha\mathbf{g}^\alpha + U_3\mathbf{g}^3 \quad ; \quad U_\alpha = \left(\mu_\delta^\gamma u_\gamma - x^3 u_{3,\delta}\right)\mu_\alpha^\delta \quad , \quad U_3 = u_3 \tag{11}$$

Figure 2 shows points A and B, and their corresponding displacements $\mathbf{U}$ and $\mathbf{u}$, respectively. The geometric interpretations for $U_\alpha\mathbf{g}^\alpha$ and $U_3\mathbf{g}^3$ are schematically shown in Figure 3, in which point A undergoes displacements U_α parallel to the shell mid-surface and a displacement U_3 normal to the mid-surface. Similarly, the contravariant components of the displacement are related to those of point B on the middle surface through

$$\mathbf{U} = U^\alpha\mathbf{g}_\alpha + U^3\mathbf{g}_3 \quad , U^\alpha = U_\beta g^{\alpha\beta} = \left(\mu_\delta^\gamma u_\gamma - x^3 u_{3,\delta}\right)\mu_\beta^\delta g^{\alpha\beta} \quad , U^3 = u^3 = u_3 \tag{12a-c}$$

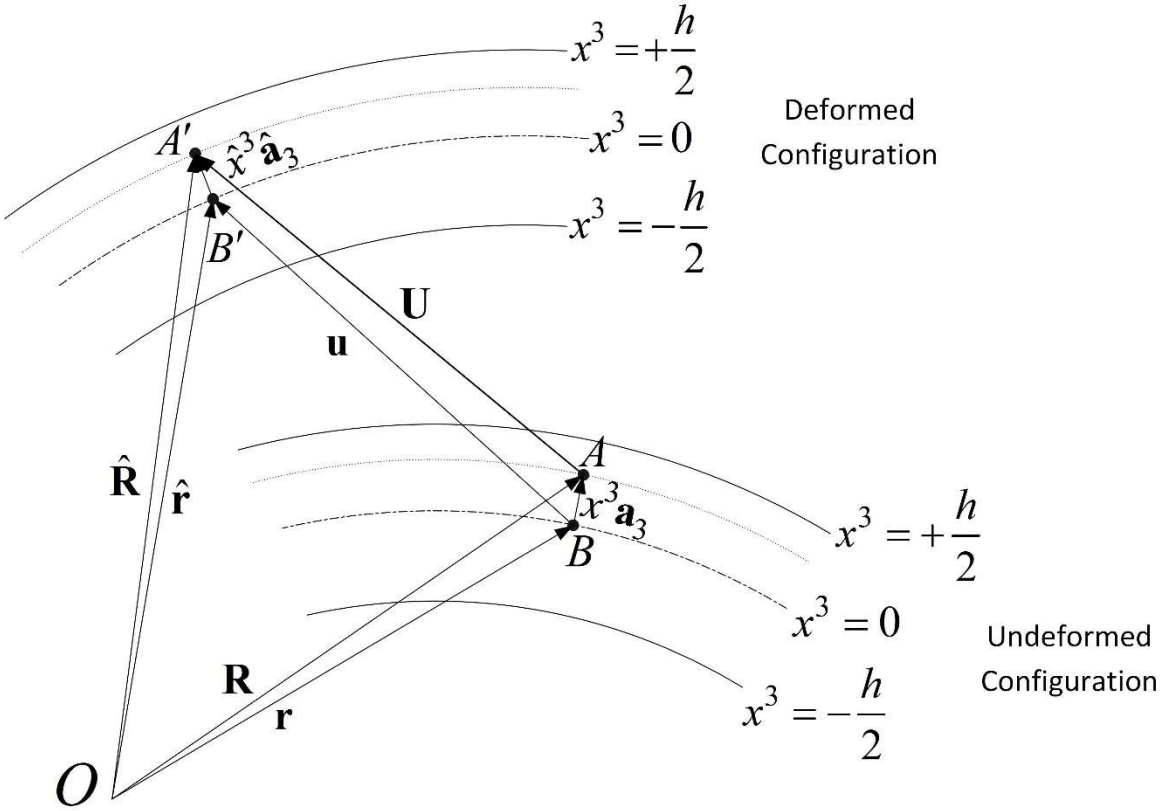

Figure 2- Deformed and Un-deformed Configurations of a Thin Shell

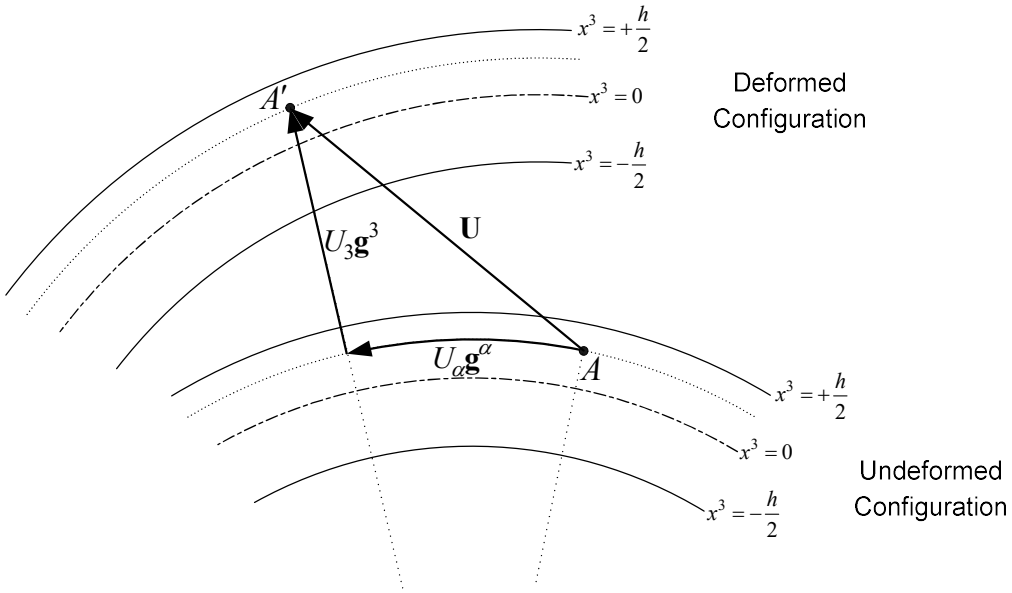

Figure 3 - Displacement of a generic point within the shell

2.4 **Stress-Strain Relationship**

For elastic materials, stress tensor σ^{ij} $(i, j = 1,2,3)$ for a point at a distance x^3 from the middle surface $(-h/2 \le x^3 \le h/2)$ is related to the corresponding strain tensor η_{lm} $(l, m = 1,2,3)$ through $\sigma^{ij} = E^{ijlm}\eta_{lm}$ (e.g., Flugge [5]), in which E^{ijlm} is the fourth order constitutive elastic tensor. For thin shells, where the stresses perpendicular to the middle surface are negligible, the number of non-zero stress components reduces from nine to four and the stress-strain relationships reduce to

$$\sigma^{\alpha\beta} = E^{\alpha\beta\lambda\delta}\eta_{\lambda\delta} \quad , \quad (\alpha, \beta, \lambda, \delta = 1,2) \tag{13}$$

Under linear elastic isotropy, the constitutive tensor can be shown [41] to take the form

$$E^{\alpha\beta\lambda\delta} = \frac{E}{2(1+\nu)}\left[g^{\alpha\lambda}g^{\beta\delta} + g^{\alpha\delta}g^{\beta\lambda} + \frac{2\nu}{1-\nu} g^{\alpha\beta}g^{\lambda\delta} \right] \tag{14}$$

in which E is the Modulus of elasticity and ν is Poisson's ratio.

2.5 **Hamilton Principle for Thin Shells of General Geometries**

According to Hamilton's principle, the variation $\delta\prod$ of the mechanical energy is given by

$$\int_{t_1}^{t_2} \delta\prod dt = \int_{t_1}^{t_2} \delta(T^* - V^*)dt + \int_{t_1}^{t_2} \delta W^* dt = 0 \tag{15}$$

in which all time integrations are performed over an arbitrary period starting from time t_1 to time t_2 and T^*, V^* and W^* are the kinetic energy, internal strain energy and external work in the system, respectively, and are given by

$$\delta T^* = \int_V \rho \dot{U}^i \delta \dot{U}_i dV \ , \quad \delta V^* = \int_V E^{ijkl}\eta_{kl}\delta\eta_{ij} dV \ , \quad \delta W^* = \int_V F^i \delta U_i dV \tag{16a-c}$$

in which integrations are over the volume V and symbols F^i denote the contravariant components of the applied forces. From Eq. 16a-c, by substituting into Eq. 15, integrating by parts the kinetic energy terms with respect to time, and using the relation $U_\alpha|_\beta = U_\alpha||_\beta - U_3 b_{\alpha\beta}$ (in which, symbol $||$ denotes the covariant derivative components of the

263 preceding argument with respect to x^{α}, i.e. $U_{\alpha}\|_{\beta}=U_{\alpha,\beta}-U_{\gamma}\Gamma^{\gamma}_{\alpha\beta}$) in the internal strain energy

264 integral term and integrating by parts with respect to x^{β} yields [41]

$$
\begin{aligned}
\int_{t_1}^{t_2}\delta\prod dt=&\left[\int_V \dot{U}^i\rho\delta U_i dV\right]_{t_1}^{t_2}+\int_{t_1}^{t_2}\left\{-\int_V \ddot{U}^i\rho\delta U_i dV dt\right.\\
&-\int_A\left[\tfrac{1}{2}E^{\alpha\beta\lambda\delta}\left(U_{\lambda}\|_{\delta}+U_{\delta}\|_{\lambda}-2U_3 b_{\lambda\delta}\right)\delta U_{\alpha}\right]_0^{x_{\beta}} dA\\
&+\int_V\left[\tfrac{1}{2}E^{\alpha\beta\lambda\delta}\left(U_{\lambda}\|_{\delta\beta}+U_{\delta}\|_{\lambda\beta}-2U_{3,\beta}b_{\lambda\delta}-2U_3 b_{\lambda\delta}\|_{\beta}\right)\right.\\
&\qquad\left.+\tfrac{1}{2}\left(E^{\alpha\beta\lambda\delta}\|_{\beta}\right)\left(U_{\lambda}\|_{\delta}+U_{\delta}\|_{\lambda}-2U_3 b_{\lambda\delta}\right)\right]\delta U_{\alpha}dV\\
&+\int_V\tfrac{1}{2}E^{\alpha\beta\lambda\delta}\left(U_{\lambda}\|_{\delta}+U_{\delta}\|_{\lambda}-2U_3 b_{\lambda\delta}\right)\left(b_{\alpha\beta}\delta U_3\right)dV\\
&\left.+\int_V F^i\delta U_i dV\right\}dt=0
\end{aligned}
\tag{17}
$$

265

266 Equation 17 is the variational form of the mechanical energy for a thin shell with general
267 curvature. The theory can be specialized to shells with specific geometries. In this context, the
268 present paper aims at specializing Eq. 17 to circular cylindrical shells. Readers interested in
269 the application of the theory to other shell geometries are referred to [41], where it has been
270 specialized to toroidal shells.

271 3. Special Case: Circular Cylindrical Thin Shells (CCTS)

272 3.1 Geometric properties

273 Position vector $\mathbf{r}$ for a general point lying on the middle surface of a circular cylinder is
274 expressed in terms of unit vectors $\vec{\mathbf{I}}_i$ in the Cartesian coordinate system χ^i (Figure 4). In terms
275 of the curvilinear coordinates system x^i, it takes the form

276 $$\mathbf{r}\left(x^1,x^2,t\right)=x^1\vec{\mathbf{I}}_1+R\sin\left(x^2/R\right)\vec{\mathbf{I}}_2+R\cos\left(x^2/R\right)\vec{\mathbf{I}}_3 \tag{18}$$

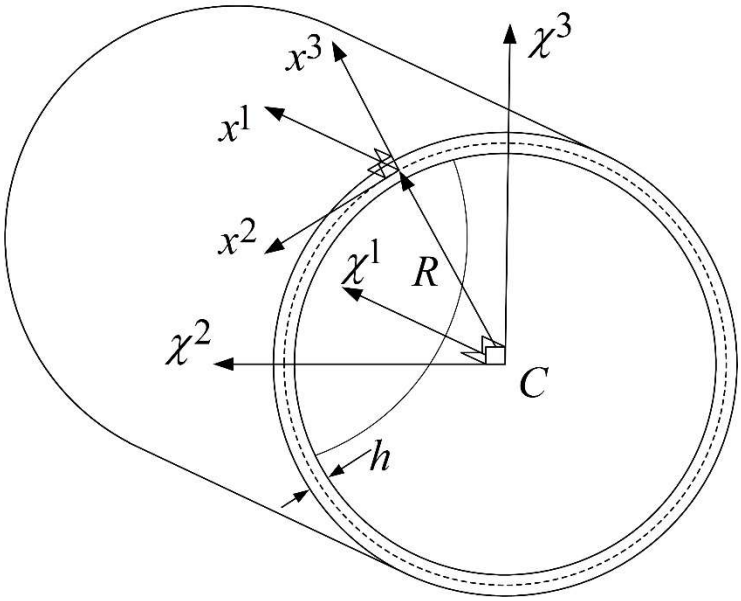

277
278 **Figure 4 - Cartesian and Curvilinear Coordinates**

279 From this point, symbols (x,s,z) will be used instead of (x^1,x^2,x^3) for clarity. The non-zero
280 components of the covariant and contravariant base vectors for a surface parallel to the mid-
281 surface lying within the shell can be shown [41] to be

282
$$\begin{array}{lll} \mathbf{g}_1=\vec{\mathbf{j}}_1 & , \ \mathbf{g}_2=(1+z/R)\,\vec{\mathbf{j}}_2 & , \ \mathbf{g}_3=\vec{\mathbf{j}}_3 \\ \mathbf{g}^1=\vec{\mathbf{j}}^1 & , \ \mathbf{g}^2=(1+z/R)^{-1}\,\vec{\mathbf{j}}^2 & , \ \mathbf{g}^3=\vec{\mathbf{j}}^3 \end{array} \tag{19}$$

283 where $\vec{\mathbf{j}}_i$ and $\vec{\mathbf{j}}^i$ are the covariant and contravariant unit vectors associated with base vectors
284 $\mathbf{g}_i$ and $\mathbf{g}^i$, respectively. The non-zero covariant and contravariant components of the metric
285 tensor are

286
$$g_{11}=g_{33}=g^{11}=g^{33}=1 \ , \ g_{22}=(1+z/R)^2 \ , \ g^{22}=(1+z/R)^{-2} \tag{20}$$

287 Also, the non-zero covariant and mixed components of the curvature tensor for a general
288 surface within the shell that is parallel to the middle surface are $b_{22}=-(1+z/R)/R$ and
289 $b_2^2=-1/R(1+z/R)$, respectively. Finally, the volume of an infinitesimal volumetric element
290 is $dV=(1+z/R)\,dzdsdx$.

3.2 **Displacements in terms of mid-surface displacements**

Considering the geometric properties obtained in Section 3.1 , the covariant and contravariant displacement components are expressed as

$$\begin{aligned} &U_1 = u - zw_{,1} \quad , \quad U_2 = \left(1+z/R\right)^2 v - z\left(1+z/R\right) w_{,2} \quad , \quad U_3 = w \\ &U^1 = u - zw_{,1} \quad , \quad U^2 = v - z\left(1+z/R\right)^{-1} w_{,2} \quad , \quad U^3 = w \end{aligned} \tag{21a-f}$$

where symbols (u,v,w) have been used instead of (u_1,u_2,u_3) for clarity. It is noted that the covariant and contravariant components of the displacements become identical at the middle surface $z=0$, i.e., $U_i\left(z=0\right) = U^i\left(z=0\right)$.

3.3 **Strain-displacement relations**

By specializing the strain displacement relations in Eq. 7a, to cylindrical shells (e.g., [41]) one obtains

$$\eta_{\alpha\beta} = \tfrac{1}{2}\left(\mu_\alpha^\delta \mu_\delta^\gamma u_{\gamma,\beta} - z\,\mu_\alpha^\delta u_{3,\delta\beta} - \mu_\alpha^\gamma u_3 \bar{b}_{\gamma\beta} + \mu_\beta^\delta \mu_\delta^\gamma u_{\gamma,\alpha} - z\,\mu_\beta^\delta u_{3,\delta\alpha} - \mu_\beta^\gamma u_3 \bar{b}_{\gamma\alpha}\right) \tag{22}$$

Prescribing the shifter tensor μ_α^δ and the curvature tensor of the middle surface $\bar{b}_{\gamma\beta}$, introduced in Sec. 2.1 , for CCTSs and substituting into Eq. 22 yields the corresponding covariant strain tensor. The physical components of the strain tensor, denoted subsequently by a tilda, can be expressed as

$$\begin{aligned} &\tilde{\eta}_{11} = u_{,1} - zw_{,11} \\ &\tilde{\eta}_{22} = v_{,2} + \frac{w}{R\left(1+z/R\right)} - \frac{zw_{,22}}{\left(1+z/R\right)} \\ &\tilde{\eta}_{12} = \tilde{\eta}_{21} = \frac{1}{2}\left\{\frac{u_{,2}}{\left(1+z/R\right)} + \left(1+z/R\right)v_{,1} - z\left[1+\frac{1}{\left(1+z/R\right)}\right]w_{,12}\right\} \end{aligned} \tag{23a-c}$$

3.4 **Components of Constitutive Tensor**

Given the components of the metric tensors (Eqs.20), by substituting into the elastic constitutive tensor in Eq.14, one recovers the following expressions for non-zero components of the constitutive tensor

$$E^{1111}=\frac{E}{1-\nu^2},\qquad E^{2222}=\frac{E}{\left(1-\nu^2\right)\left(1+z/R\right)^4},\quad E^{1122}=E^{2211}=\frac{E\nu}{\left(1-\nu^2\right)\left(1+z/R\right)^2},$$
$$E^{1212}=E^{1221}=E^{2112}=E^{2121}=\frac{E\left(1-\nu\right)}{2\left(1-\nu^2\right)\left(1+z/R\right)^2} \tag{24a-d}$$

3.5 **Hamilton Principle for CCTS**

From Eqs. 21 and 24, by substituting into the variation of the Hamilton's principle in Eq. 17, integrating with respect to z, grouping like-terms and integrating by parts with respect to x and s yields [41]

$$\begin{aligned}\int_{t_1}^{t_2}\delta\prod dt=\int_{t_1}^{t_2}\Bigg\langle\int_s\frac{Eh}{1-\nu^2}\Big[&\left({}_1^1\bar{H}u_{,1}+{}_2^1\bar{H}v_{,2}+{}_3^1\bar{H}w+{}_4^1\bar{H}w_{,11}\right)\delta u\\&+\left({}_1^2\bar{H}u_{,2}+{}_2^2\bar{H}v_{,1}+{}_3^2\bar{H}w_{,12}\right)\delta v\\&+\left({}_1^3\bar{H}u_{,11}+{}_2^3\bar{H}u_{,22}+{}_3^3\bar{H}v_{,12}+{}_4^3\bar{H}w_{,111}+{}_5^3\bar{H}w_{,122}+{}_6^3\bar{H}\ddot{u}+{}_7^3\bar{H}\ddot{w}_{,1}+{}_8^3\bar{H}f^{xw}\right)\delta w\\&+\left({}_1^4\bar{H}u_{,1}+{}_2^4\bar{H}v_{,2}+{}_3^4\bar{H}w_{,11}+{}_4^4\bar{H}w_{,22}\right)\delta w_{,1}\Big]_0^L ds\\+\int_A\frac{Eh}{1-\nu^2}\Big[&\left({}_1^1\bar{G}u_{,11}+{}_2^1\bar{G}u_{,22}+{}_3^1\bar{G}v_{,12}+{}_4^1\bar{G}w_{,1}+{}_5^1\bar{G}w_{,111}+{}_6^1\bar{G}w_{,122}\right.\\&\left.+{}_7^1\bar{G}\ddot{u}+{}_8^1\bar{G}\ddot{w}_{,1}+{}_9^1\bar{G}f^{xu}\right)\delta u\\&+\left({}_1^2\bar{G}u_{,12}+{}_2^2\bar{G}v_{,11}+{}_3^2\bar{G}v_{,22}+{}_4^2\bar{G}w_{,2}+{}_5^2\bar{G}w_{,112}+{}_a^2\bar{G}w_{,222}+{}_6^2\bar{G}\ddot{v}+{}_7^2\bar{G}\ddot{w}_{,2}+{}_8^2\bar{G}f^{sv}\right)\delta v\\&+\left({}_1^3\bar{G}u_{,1}+{}_2^3\bar{G}v_{,2}+{}_3^3\bar{G}w+{}_a^3\bar{G}w_{,11}+{}_4^3\bar{G}w_{,22}+{}_5^3\bar{G}u_{,111}+{}_6^3\bar{G}u_{,122}+{}_7^3\bar{G}v_{,112}+{}_b^3\bar{G}w_{,222}\right.\\&+{}_8^3\bar{G}w_{,1111}+{}_9^3\bar{G}w_{,1122}+{}_{10}^3\bar{G}w_{,2222}+{}_{11}^3\bar{G}\ddot{w}+{}_{12}^3\bar{G}\ddot{w}_{,11}+{}_{13}^3\bar{G}\ddot{w}_{,22}+{}_{14}^3\bar{G}\ddot{u}_{,1}+{}_{15}^3\bar{G}\ddot{v}_{,2}\\&\left.+{}_{16}^3\bar{G}f_{,1}^{xw}+{}_{17}^3\bar{G}f_{,2}^{sw}+{}_{18}^3\bar{G}f^{zw}\right)\delta w\Big]dsdx\Bigg\rangle dt=0\end{aligned} \tag{25}$$

where coefficients ${}_1^1\bar{G}$ - ${}_{18}^3\bar{G}$ and ${}_1^1\bar{H}$ - ${}_4^4\bar{H}$, depend on the parameter

$$\Phi=\Phi\left(h/R\right)=\left(R/h\right)\ln\left[\left(2+h/R\right)/\left(2-h/R\right)\right] \tag{26}$$

and are defined in Appendix A. The terms $f^{xu},f^{xw},f^{sv},f^{sw},f^{zw}$ arising in Eq. 25 are related to the physical force components per unit volume p^x,p^s,p^z and are provided in Appendix B.

3.6 **Discussion**

The field equations and corresponding boundary conditions for a CCTS can be obtained from Eq. 25 through integration by parts. The details and relevant equations are provided in Appendix B, where the boundary conditions are given by Eq. B.2 and the field equations are given by Eq. B.3. These are entirely consistent with the assumptions postulated in Section 1.2 . In order to recover simpler approximate forms of the field equations and cast the present formulation in a format comparable to other CCTS theories, the logarithmic function (Eq. 26) appearing in Eq. 25 is replaced by a truncated Taylor series expansion

$$\Phi\left(h/R\right) \approx 1+\left(h/R\right)^2/12+\left(h/R\right)^4/80+\ \cdots \tag{27}$$

By omitting all time dependent terms, retaining the traction terms f^{xu}, f^{sv}, f^{zw} , omitting the terms f^{xw}, f^{sw} and using the series approximation in Eq. 27 up to the second term, one recovers the field equations in Flugge's theory [4] as a special case of the present formulation. A simpler version of the present theory can also be obtained by adopting the approximation $1+z/R \approx 1$, in the strain displacement expressions (Eqs. 23a-c), the base vector expressions, and the Jacobian. The resulting field equations are found to coincide with those of the DMV theory [7]. Finally, as $\left(1+z/R\right) \to 1$, the present theory, the Flugge theory and the DMV are found to converge to the same field equations.

In contrast to other thin-shell theories known to the authors, the present formulation treats the applied loads as body forces, and thus, is able to capture the spatial variations of the loads along all three dimensions. Mid-surface tractions, line loads, and point loads can all be treated as body forces by using the Dirac delta and Heaviside functions.

3.7 **Comparison**

Table 1 compares the strain expressions adopted in the past theories to those of the present study. All theories are in agreement regarding the expression $\tilde{\eta}_{11} = u_{,1} - zw_{,11}$ for the longitudinal strain. The Jacobian determinant is taken as unity in all theories except the present and Flugge's theories, in which the Jacobian is $\left(1+z/R\right)^2$. Table 1 provides a comparison of the circumferencial and shear strains $\tilde{\eta}_{22}$ and $\tilde{\eta}_{12}$ as given in various theories. Strain

expressions based on Flugge's theory are observed to become in exact agreement with those of the present theory when the approximation $\Phi(h/R) \approx 1+(h/R)^2/12$ is adopted. The Novozhilov strain expressions can be obtained from the strains of the present theory by applying the approximations $\Phi(h/R) \approx 1+(h/R)^2/12$ and $1+z/R \approx (1-z/R)^{-1}$, while the DMV strain expressions can be recovered from the strains of the present theory by applying the approximations $\Phi(h/R) \approx 1+(h/R)^2/12$ and $1+z/R \approx 1$. In contrast, strain expressions in the theories of Timoshenko [1], Saada [6], Morley-Koiter [7] and Niordson [7] include additional terms that do not arise in the present tensor-based approach. Such terms stem from additional approximations that have been introduced in these theories, but avoided in the present tensorial treatment.

Table 1– Comparing strain-displacement expressions in various thin shell theories

Theory	Strain Expressions	
	$\tilde{\eta}_{22}$	$\tilde{\eta}_{12}$
Flugge's theory [4] & Present Theory with approximation $\Phi(h/R) \approx 1+(h/R)^2/12$	$v_{,2}+\frac{1}{R+z}w-z\frac{R}{R+z}w_{,22}$	$\frac{1}{2}\left(\frac{R}{R+z}u_{,2}+\frac{R+z}{R}v_{,1}-z\frac{2R+z}{R+z}w_{,12}\right)$
Novozhilov [2] & Present Theory with approximations $\Phi(h/R) \approx 1+(h/R)^2/12$ and $1+z/R \approx (1-z/R)^{-1}$	$v_{,2}+\frac{1}{R}\frac{R-z}{R}w-zw_{,22}$	$\frac{1}{2}\left(\frac{R-z}{R}u_{,2}+\frac{R+z}{R}v_{,1}-2zw_{,12}\right)$
Saada [6]	$\frac{R+z}{R}v_{,2}+\frac{1}{R}w-zw_{,22}$	$\frac{1}{2}\left(u_{,2}+\frac{R+z}{R}v_{,1}-2zw_{,12}\right)$
Timoshenko [1]	$\frac{R+z}{R}v_{,2}+\frac{1}{R}w-zw_{,22}$	$\frac{1}{2}\left(u_{,2}+\frac{R+2z}{R}v_{,1}-2zw_{,12}\right)$
Morley-Koiter [7] & Niordson [7]	$\frac{R+2z}{R}v_{,2}+\frac{1}{R}\frac{R+z}{R}w-zw_{,22}$	$\frac{1}{2}\left(u_{,2}+\frac{R+2z}{R}v_{,1}-2zw_{,12}\right)$
DMV [7] & Present Theory with approximations $\Phi(h/R) \approx 1$ and $1+z/R \approx 1$	$v_{,2}+\frac{1}{R}w-zw_{,22}$	$\frac{1}{2}\left(u_{,2}+v_{,1}-2zw_{,12}\right)$

The presence of such differences at the strain expression stage, combined with other simplifications and approximations, leads to differences in their corresponding field equations

and boundary conditions. In order to conduct a comparative study, irrespective of the CCTS theory adopted, the equilibrium conditions can be cast into the following generic form

$$u_{,11}+\boxed{\alpha_{1.1}}\frac{1-\nu}{2}u_{,22}+\frac{1+\nu}{2}v_{,12}+\frac{\nu}{R}w_{,1}-\boxed{\alpha_{1.2}}\frac{h^2}{12R}w_{,111}+\boxed{\alpha_{1.3}}\frac{1-\nu}{2}w_{,122}$$
$$-\rho\frac{1-\nu^2}{E}\left(\ddot{u}-\boxed{\alpha_{1.4}}\frac{h^2}{12R}\ddot{w}_{,1}\right)+f^{xu}=0 \tag{365}$$

$$\frac{1+\nu}{2}u_{,12}+\boxed{\alpha_{2.1}}\frac{1-\nu}{2}v_{,11}+\boxed{\alpha_{2.2}}v_{,22}+\frac{1}{R}w_{,2}-\boxed{\alpha_{2.3}}\frac{h^2}{12R}w_{,112}-\boxed{\alpha_{2.4}}\frac{h^2}{12R}w_{,222}$$
$$-\rho\frac{1-\nu^2}{E}\left(\boxed{\alpha_{2.5}}\ddot{v}-\boxed{\alpha_{2.6}}\frac{h^2}{6R}\ddot{w}_{,2}\right)+f^{sv}=0 \tag{366}$$

$$\frac{\nu}{R}u_{,1}+\frac{1}{R}v_{,2}+\boxed{\alpha_{3.1}}\frac{1}{R^2}w+\boxed{\alpha_{3.2}}w_{,11}+\boxed{\alpha_{3.3}}w_{,22}-\boxed{\alpha_{3.4}}\frac{h^2}{12R}u_{,111}+\boxed{\alpha_{3.5}}\frac{1-\nu}{2}u_{,122}$$
$$-\boxed{\alpha_{3.6}}\frac{h^2}{12R}v_{,112}+\boxed{\alpha_{3.7}}w_{,222}+\frac{h^2}{12}w_{,1111}+\boxed{\alpha_{3.8}}w_{,1122}+\boxed{\alpha_{3.9}}w_{,2222}$$
$$-\rho\left(1-\nu^2\right)/E\left[\ddot{w}-\boxed{\alpha_{3.10}}\frac{h^2}{12}\left(\ddot{w}_{,11}+\ddot{w}_{,22}\right)+\boxed{\alpha_{3.11}}\frac{h^2}{12R}\left(\ddot{u}_{,1}+2\ddot{v}_{,2}\right)\right]$$
$$+\left(1-\nu^2\right)/Eh\left(-f_{,1}^{xw}-f_{,2}^{sw}+f^{zw}\right)=0 \tag{367}$$

where coefficients $\alpha_{i.j}$ are theory-dependent and are defined in Table 2. As observed, the adoption of various assumptions/approximations in various theories, has led to the elimination of terms in some cases (e.g., $-\boxed{\alpha_{1.2}}\left(h^2/12R\right)w_{,111}$, $-\boxed{\alpha_{3.4}}\left(h^2/12R\right)u_{,111}$ and $\boxed{\alpha_{3.5}}\left[\left(1-\nu\right)/2\right]u_{,122}$ for Timoshenko, Novozhilov and Saada), and to the emergence of additional terms in other cases (e.g., $\boxed{\alpha_{2.4}}w_{,222}$, $\boxed{\alpha_{3.2}}w_{,11}$ and $\boxed{\alpha_{3.7}}w_{,222}$ for Timoshenko, Novozhilov and Saada), when compared to the present treatment. Such approximations/simplifications have only affected the magnitude of coefficients of other terms in some cases.

Table 2 - Comparison of field equation coefficients $\alpha_{i.j}$ for various CCTS theories

F.E.s	Present Theory	Flugge [4]	Timoshenko [1], Novozhilov [2], Saada [6],	Morley-Koiter [7], Niordson [7], DMV [7]
$\alpha_{1.1}$	Φ	$\left(1+h^2/12R^2\right)$	1	1
$\alpha_{1.2}$	1	1	0	0

$\alpha_{1.3}$	$R(\Phi-1)$	$h^2/12R$	0	0
$\alpha_{1.4}$	1	-	0	0
$\alpha_{2.1}$	$1+h^2/4R^2$	$1+h^2/4R^2$	$1+h^2/3R^2$ [Take $(1+h^2/12R^2)$ for Timoshenko]	1
$\alpha_{2.2}$	1	1	$1+h^2/12R^2$	1
$\alpha_{2.3}$	$(3-\nu)/2$	$(3-\nu)/2$	1 [Take $(2-\nu)$ for Novozhilov]	0
$\alpha_{2.4}$	0	0	1	0
$\alpha_{2.5}$	$1+h^2/12R^2$	$1+h^2/12R^2$	-	1
$\alpha_{2.6}$	1	1	-	0
$\alpha_{3.1}$	Φ	$1+h^2/12R^2$	1	$1+h^2/12R^2$ [Take unity for DMV]
$\alpha_{3.2}$	0	0	0	$1+h^2/6R^2$ [Vanishes for DMV]
$\alpha_{3.3}$	$2(\Phi-1)$	$h^2/6R^2$	0	$h^2/6R^2$ [Vanishes for DMV]
$\alpha_{3.4}$	1	1	0	0
$\alpha_{3.5}$	$R(\Phi-1)$	$h^2/12R$	0	0
$\alpha_{3.6}$	$(3-\nu)/2$	$(3-\nu)/2$	$(2-\nu)$ [Take unity for Saada]	0
$\alpha_{3.7}$	0	0	$h^2/12R$	0
$\alpha_{3.8}$	$(3+\nu)h^2/24+$ $R^2(\Phi-1)(1-\nu)/2$	$h^2/6$	$h^2/6$	$h^2/6$
$\alpha_{3.9}$	$R^2(\Phi-1)$	$h^2/12$	$h^2/12$	$h^2/12$
$\alpha_{3.10}$	1	-	-	1
$\alpha_{3.11}$	1	-	-	0
$\alpha_{3.12}$	1	-	-	1

Similarly, the boundary terms have been cast into the following generic form.

$$\left(u_{,1}+\nu v_{,2}+\frac{\nu}{R}w-\boxed{\beta_{1.1}}\frac{h^2}{12R}w_{,11}\right)\delta u$$

$$\left(u_{,2}+\boxed{\beta_{2.1}}v_{,1}-\frac{h^2}{4R}w_{,12}\right)\delta v$$

$$\left(\boxed{\beta_{3.1}}\frac{h^2}{12R}u_{,11}-\boxed{\beta_{3.2}}\frac{1-\nu}{2}u_{,22}+\boxed{\beta_{3.3}}\frac{h^2}{12R}v_{,12}-\frac{h^2}{12}w_{,111}-\boxed{\beta_{3.4}}\frac{h^2}{12}w_{,122}\right)\delta w$$

$$\left(\boxed{\beta_{4.1}}\frac{h^2}{12R}u_{,1}+\boxed{\beta_{4.2}}\frac{h^2}{12R}\nu v_{,2}-\frac{h^2}{12}w_{,11}-\frac{h^2}{12}\nu w_{,22}\right)\delta w_{,1}$$

Table 3 provides coefficients $\beta_{i.j}$ for the present theory and those of Flugge, Timoshenko and DMV.

Table 3 - Comparison of field equation coefficients $\beta_{i.j}$ for various CCTS theories

B.C.s	Present Theory	Flugge	Timoshenko	DMV
$\beta_{1.1}$	1	1	0	0
$\beta_{2.1}$	$\left(1+h^2/4R^2\right)$	$\left(1+h^2/4R^2\right)$	$2/3$	0
$\beta_{3.1}$	1	1	0	0
$\beta_{3.2}$	$R(\Phi-1)$	$h^2/12R$	0	0
$\beta_{3.3}$	$(3-\nu)/2$	$(3-\nu)/2$	1	0
$\beta_{3.4}$	$\left[(3-\nu)/2+(\Phi-1)(1-\nu)6R^2/h^2\right]$	$(2-\nu)$	1	$(2-\nu)$
$\beta_{4.1}$	1	1	0	0
$\beta_{4.2}$	1	1	1	0

3.8 **Steady State Analysis under Harmonic Forces**

Consider a CCTS under general harmonic force per unit volume $\left[p^x(x,s,z,t),p^s(x,s,z,t),p^z(x,s,z,t)\right]=\left[\overline{p}^x(x,s,z),\overline{p}^s(x,s,z),\overline{p}^z(x,s,z)\right]\mathrm{Re}\left(e^{i\overline{\omega}t}\right)$, with an exciting frequency $\overline{\omega}$. It is possible to express the force functions using double Fourier series with N circumferential modes and K longitudinal modes yielding:

$$\begin{Bmatrix} p^x \\ p^s \\ p^z \end{Bmatrix} = \sum_{n=-N}^{N} \sum_{k=-K}^{K} \left[\begin{Bmatrix} p_{nk}^x(z) \\ p_{nk}^s(z) \\ p_{nk}^z(z) \end{Bmatrix} e^{2\pi ikx/L} e^{ins/R} \right] \mathrm{Re}\left(e^{i\bar{\omega}t}\right) \quad ,$$

393 (28a-b)

$$\begin{Bmatrix} p_{nk}^x(z) \\ p_{nk}^s(z) \\ p_{nk}^z(z) \end{Bmatrix} = \int_{s=0}^{s=2\pi R} \int_{x=0}^{x=L} \begin{Bmatrix} \overline{p}^x(x,s,z) \\ \overline{p}^s(x,s,z) \\ \overline{p}^z(x,s,z) \end{Bmatrix} e^{-2\pi ikx/L} e^{-ins/R} dxds$$

394 in which, each applied force component is expressed in terms of its Fourier series expansion
395 in x and s. From Eq. 28, by substituting into Equations B.1a-e and integrating over the
396 thickness, one obtains

$$\begin{Bmatrix} f^{xu} \\ f^{sv} \\ f^{zw} \\ f^{xw} \\ f^{sw} \end{Bmatrix} = \left[\sum_{n=-N}^{N} \sum_{k=-K}^{K} \begin{Bmatrix} f_{nk}^{xu} \\ f_{nk}^{sv} \\ f_{nk}^{zw} \\ f_{nk}^{xw} \\ f_{nk}^{sw} \end{Bmatrix} e^{2\pi ikx/L} e^{ins/R} \right] \mathrm{Re}\left(e^{i\bar{\omega}t}\right) \quad ,$$

397 (29a-b)

$$\begin{Bmatrix} f_{nk}^{xu} \\ f_{nk}^{sv} \\ f_{nk}^{zw} \\ f_{nk}^{xw} \\ f_{nk}^{sw} \end{Bmatrix} = \int_{z=-\frac{h}{2}}^{z=+\frac{h}{2}} \begin{Bmatrix} p_{nk}^x(z)\left(1+z/R\right) \\ p_{nk}^s(z)\left(1+z/R\right)^2 \\ p_{nk}^z(z)\left(1+z/R\right) \\ p_{nk}^x(z)\,z\left(1+z/R\right) \\ p_{nk}^z(z)\,z\left(1+z/R\right) \end{Bmatrix} dz$$

398 For a given load, constants f^{xu}, f^{sv}, f^{zw}, f^{xw} and f^{sw} are determined and a procedure
399 similar to that reported in [24] is then used to provide a closed form solution for each of the
400 theories developed. The corresponding steady state displacements are expressed in the
401 following form.

$$u(x,s,t)=\bar{u}(x,s)e^{i\bar{\omega}t}=\sum_{n=-N}^{N}\left(\sum_{j=1}^{8}A_{nj}\bar{A}_{nj}e^{m_{nj}x}+\sum_{k=-K}^{K}R_{nk}e^{2\pi ikx/L}\right)e^{ins/R}e^{i\bar{\omega}t}$$

$$v(x,s,t)=\bar{v}(x,s)e^{i\bar{\omega}t}=\sum_{n=-N}^{N}\left(\sum_{j=1}^{8}A_{nj}\bar{B}_{nj}e^{m_{nj}x}+\sum_{k=-K}^{K}S_{nk}e^{2\pi ikx/L}\right)e^{ins/R}e^{i\bar{\omega}t} \quad (30a\text{-}c)$$

$$w(x,s,t)=\bar{w}(x,s)e^{i\bar{\omega}t}=\sum_{n=-N}^{N}\left(\sum_{j=1}^{8}A_{nj}\bar{C}_{nj}e^{m_{nj}x}+\sum_{k=-K}^{K}T_{nk}e^{2\pi ikx/L}\right)e^{ins/R}e^{i\bar{\omega}t}$$

Symbols m_{nj} are the eigenvalues and each set of symbols $\bar{A}_{nj}$, $\bar{B}_{nj}$, $\bar{C}_{nj}$ form the corresponding eigenvectors of the characteristic equation of the system related to mode n. Symbols R_{nk}, S_{nk}, T_{nk} and A_{nj} are unknown integration constants to be determined from boundary conditions (e.g., [24]).

3.9 **Examples**

In the following examples, the above solution technique is adopted to express the applied forces and displacement fields in the circumferential direction s and lomgitudinal direction x. Examining the terms in Eqs. B.2 and B.3, as well as the entries in Table 2 and Table 3 reveals that the theories of Timoshenko, Novozhilov and Saada have largely similar governing equations and boundary conditions. Thus, the theory of Timoshenko has been chosen as a representative of this group. Similarly, the DMV theory has been taken as a representative of the Morley-Koiter, Niordson and DMV group of theories given their similarity. In all examples, results based on Abaqus models are provided for comparison. Four types of elements have been used in Abaqus models depending on the problem.

- S4R: A four-noded general-purpose (thin or thick) shell element, with reduced integration and hourglass control.
- S8R: An eight-noded doubly curved thick shell element with reduced integration
- C3D8R: An eight-noded linearly interpolated brick element with reduced integration and hourglass control, and
- C3D20R: A twenty-node quadratically interpolated brick element with reduced integration.

In all examples, steel is assumed to have a density of $\rho=7850\,kg/m^3$, a modulus of elasticity of $200\,GPa$ and a Poisson's ratio of $\nu=0.3$.

3.9.1 Example 1 - Pipe under Self-Weight

A $4\,m$ long fixed-free horizontal pipe with a radius $R = 200\,mm$ and a thickness $h = 6mm$ is subjected to its self-weight. The response is obtained based on the present theory, the Flugge, Timoshenko, DMV theories, and the Abaqus shell model. In the Abaqus model, by refining the mesh from 64×200 to 128×400 S4R elements, the changes in the predicted displacements were within 0.9%, suggesting that convergence has been achieved. The static solution sought in the present problem is recovered by setting to zero the exciting frequency $\bar{\omega}$. Figure 5 provides a comparison of the longitudinal and radial displacements at the top generator of the pipe mid-surface. Nearly perfect agreement is observed among all solutions except for the DMV, which exhibits a significantly stiffer response as indicated by the lower displacements observed. A comparison of the predictions of the present and DMV theories shows a 53% difference (for a thickness $h = 6\,mm$). When the pipe thickness is reduced to $h = 3\,mm$, the difference between both solutions reduces to 22% , drops further to 6.5% for $h = 1.5\,mm$, and becomes only 3% for $h = 1\,mm$. The fact that the DMV theory adopts the approximation $(1 + z/R) \approx 1$, while the other theories do not enforce such an approximation, limits the usability of the DMV theory for very thin shells.

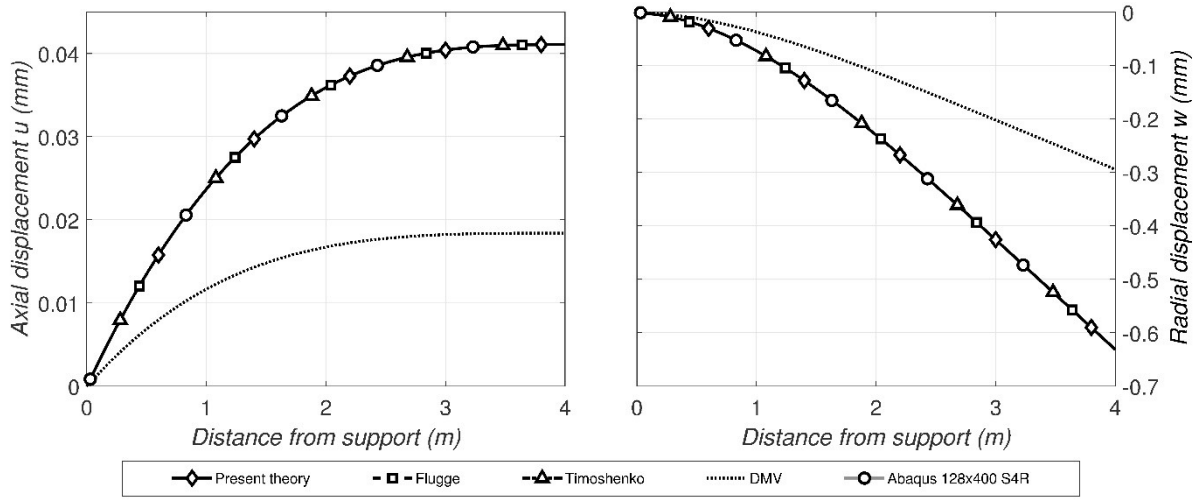

Figure 5–Comparison of longitudinal and radial displacements at the top generator

3.9.2 Example 2 - Fixed pipe under harmonic pressure

Example 1 in [24] is revisited: A pipe with span length $L = 5\,m$, radius $R = 25\,mm$, thickness $h = 5\,mm$ is fixed at both ends and is subjected to wind load traction $t^z(x,s,t) = 100\cos(s/R)\cos(\bar{\omega}t)\ kN/m^2$, where $\bar{\omega} = 200\,rad/s$, simulating a vortex shedding

447 phenomenon. Casting the applied traction in form of body forces applicable to the present
448 formulation yields $p^z = t^z\left(x,s,t\right) Dirac\left(z-h/2\right)\ N/m^3$. In addition to the present theory,
449 solutions are to be provided under the Flugge, Timoshenko, and DMV theories as well as
450 Abaqus FEA for comparisons. In the Abaqus model, by refining the mesh from 64×200 to
451 128×400 S4R elements, the change in the predicted displacements was less than 0.05%,
452 suggesting that convergence has been achieved by 64×200 mesh.

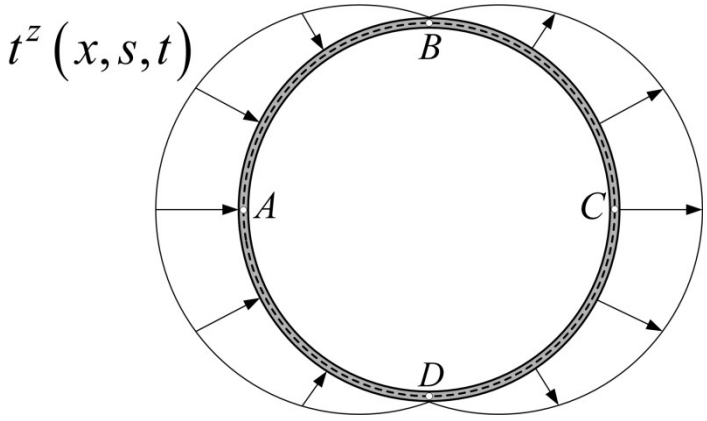

453

454 **Figure 6 - Cross-sectional distribution of the wind load.**

455 The maximum longitudinal and radial displacements at midsurface ($z=0$) take place at the
456 generators passing through points $A\,(s=0)$ and $C\,(s=\pi/4)$ and the maximum
457 circumferential midsurface displacement occurs at the generators passing through points B (
458 $s=\pi/8$) and D ($s=3\pi/8$), as shown in Figure 6. Table 4 gives the maximum displacements
459 and their respective locations as provided by the present theory and percentage differences
460 based on other solutions mentioned above. For the present problem, the predictions of the
461 present theory are indistinguishable from those of the Flugge and Timoshenko theories, while
462 the DMV solution slightly underpredicts the displacement by about 2.7%. The Abaqus
463 solution, also, is found to slightly underpredicting the displacement by less than 1%.
464

Table 4 - Comparing the displacement components at the location of their maximum

	Present theory	Difference from the present theory (%)			
		Flugge	Timoshenko	DMV	Abaqus (64×200 S4R)
$\overline{u}_A = -\overline{u}_C$ at $x = 0.21L$ $-\overline{u}_A = \overline{u}_C$ at $x = 0.79L$	$0.4410\,mm$	0.00	-0.01	2.73	0.91
$\overline{v}_B = -\overline{v}_D$ at $x = 0.5L$	$3.753\ mm$	0.00	-0.01	2.72	0.92
$\overline{w}_A = -\overline{w}_C$ at $x = 0.5L$	$-3.725\,mm$	0.00	-0.01	2.72	0.92

The distribution of longitudinal stresses σ_{xx} and transverse stresses σ_{ss} for the generator passing through point A (Figure 6) are depicted in Figure 7 and Figure 8. Flugge's theory predictions nearly coincide with those of the present solution, and the Timoshenko theory predictions are in rather close agreement. The predictions of the DMV theory are 1-3% below those based on the other theories. Although, in the present example, all four theories predict stresses in rather close agreement, this will not always be the case. For instance, if all degrees of freedom at end $x = L$ are released (turning the beam into a cantilever), the stresses predicted by the DMV are found to depart from those predicted by the Timoshenko, Flugge and present theories. Figure 9 depicts the longitudinal stress σ_{xx} along a generator passing through point A (in Figure 6) under only 20% of the magnitude of $t^z\left(x,s,t\right)$ (to keep the maximum stresses within the elastic range of the structural steel properties). The figure shows that the DMV prediction significantly departs from those of the other theories.

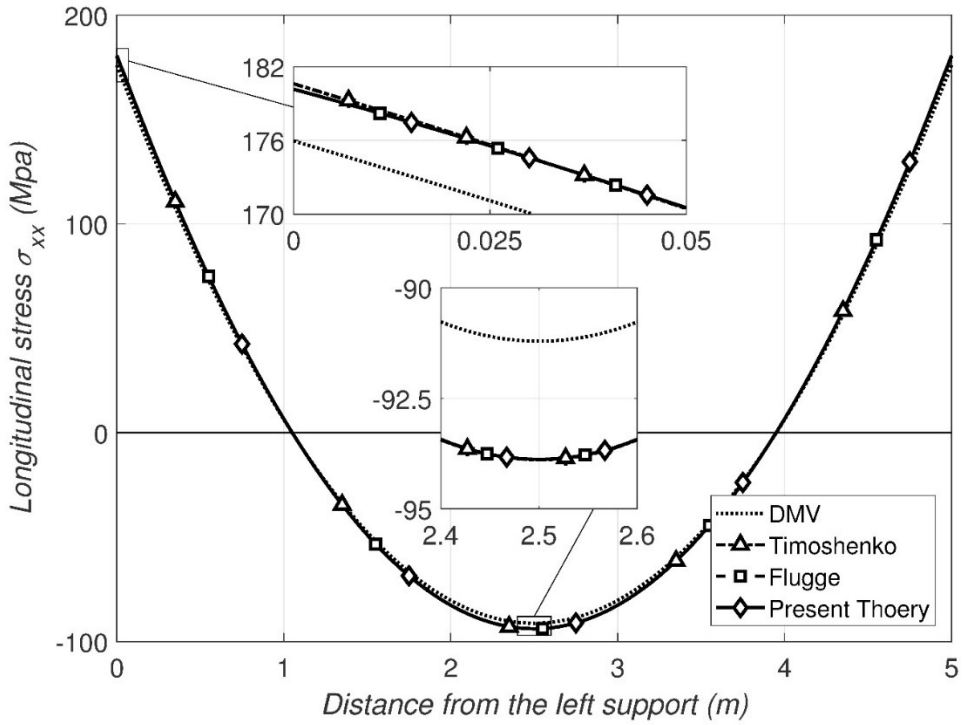

Figure 7 - Longitudinal stress (σ_{xx}) along a generator passing through point A

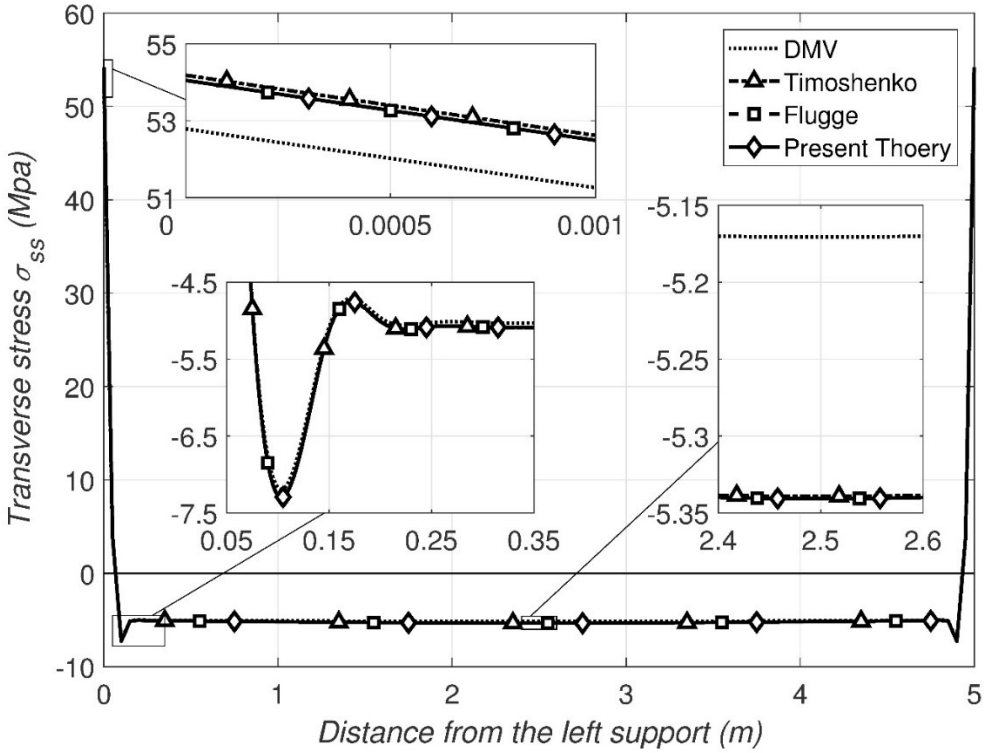

Figure 8 - Transverse stress (σ_{ss}) along a generator passing through point A

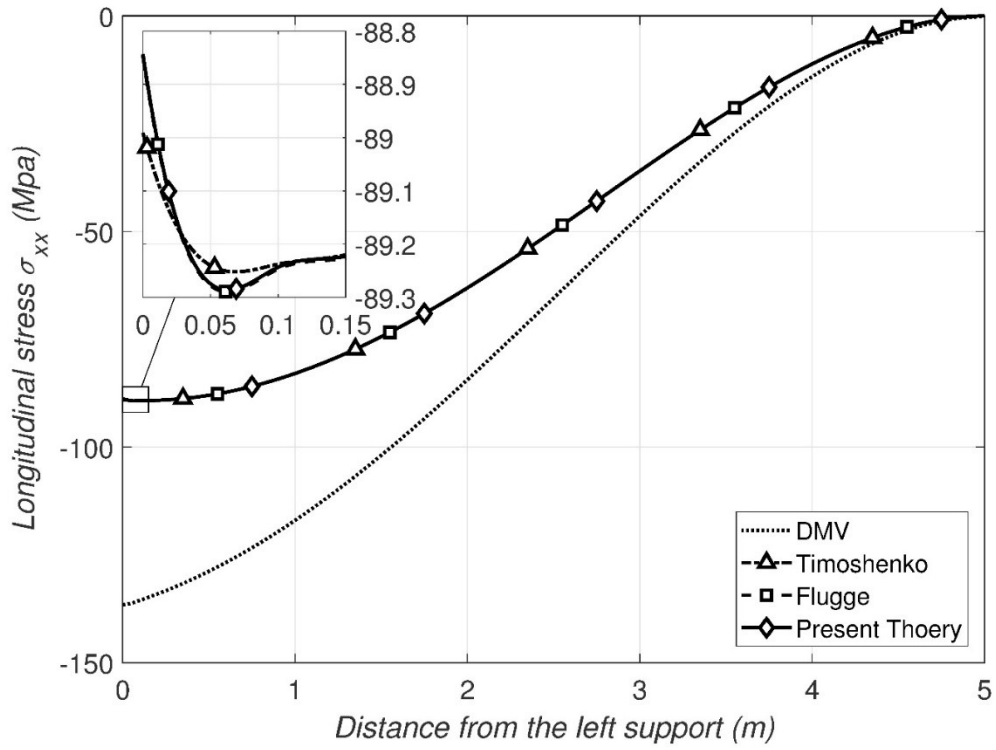

Figure 9 - Longitudinal stress (σ_{xx}) along a generator passing through point A for cantilever

The amplitudes of the radial displacements at Point A as predicted by the present solution are compared to those predicted by the Abaqus shell model for wide range of angular frequencies (Figure 10). In Abaqus, by refining the mesh from 80×255 to 160×510 S4R elements, the change in the predicted displacements was less than 0.9% for frequencies ranging from 0 to 200 rad/s, suggesting that convergence has been achieved. The radial displacement amplitudes (as identified on the scale of the left vertical axis) based on both solutions are nearly in perfect agreement and are barely distinguishable within the scale of the figure. The loci of the peak amplitudes, indicative of the natural frequencies, are also in excellent agreement with Abaqus predictions. Also shown on the figure is the percentage difference of the radial displacement at point A between both solutions, as identified on the scale of the right vertical axis. Except near the natural frequencies where both solutions approach infinity, or where the amplitude approaches zero, the amplitude difference is within 3%. The comparison indicates that the present theory predicts lower natural frequencies for most of the frequency range and higher amplitudes compared to Abaqus.

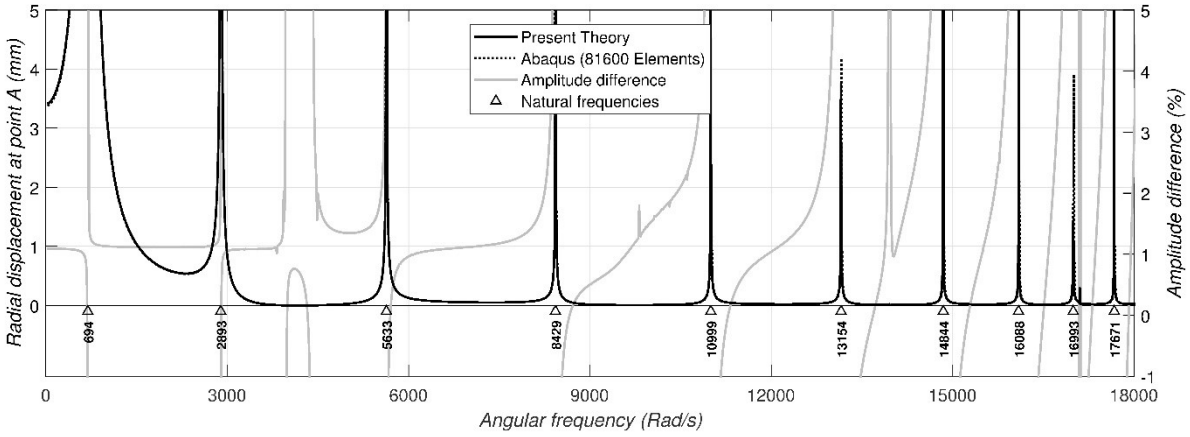

501

502 **Figure 10 – Radial amplitude versus exciting frequency**

503

504 ### 3.9.3 Example 3 - Pipe under a Point Load

505 The fixed pipe in Example 2 is set free at end $x = L$ and is subject to an inclined point load

506 $(1,1,-1)kN$ (Figure 11) along the x, s and z directions, acting at point

507 $P_0(x,s,z) = (0.7L,0,0)$.

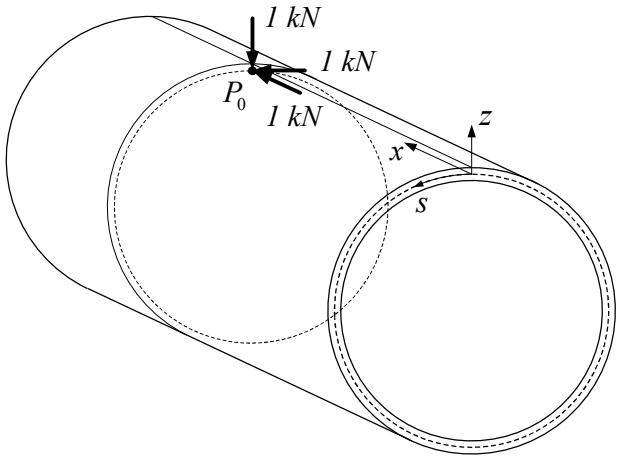

508

509 **Figure 11 – Location, magnitude and direction of the point load components**

510 The point loads can be expressed as body forces

511 $(p^x, p^s, p^z) = Dirac(x-0.7L)\,Dirac(s)\,Dirac(z)(1,1,1)kN$ and expanded as double Fourier

512 series in the x and z directions. To investigate the convergence of the solution, the number of

513 Fourier modes taken is varied ($N = K = 7, 10, 15, 20, 25$). Five Abaqus S4R shell models,

514 with uniform meshes, were conducted for comparison (16×50, 32×100, 64×200, 128×400

515 and 320×640). The four coarse meshes are uniform while the most refined mesh (320×640

) is identical to the 128×400 mesh, with a refined rectangular patch of elements in the neighborhood of the point load. The patch extends longitudinally from $x=0.6L$ to $x=0.8L$ and from $s=-\pi R/2$ to $s=\pi R/2$ in the circumferential direction and consists of 256×320 elements (instead of 64×80 elements in the 128×400 elements model), and is intended to capture localized deformations around the point load. In Abaqus, a mesh study indicated that convergence was achieved for 128×400 S4R mesh. A finer 320×640 mesh resulted only in a maximum difference of 0.23% in the displacements predicted.

The longitudinal, circumferential, and radial displacements at the generator at which the point load is applied ($s=z=0$) are respectively depicted in Figure 12 to Figure 14. As the number of Fourier terms increases in the present solution, and as the number of elements increase in the Abaqus solution, both models are observed to approach one another, albeit in the limit, both converged solutions do not exactly coincide. The rather minor differences observed arise from the fact that an exact representation of the point load requires an infinite number of modes ($N\to\infty$ & $K\to\infty$), which is unachievable as the number of modes taken has to be truncated. To confirm this hypothesis, an additional Abaqus solution is conducted (denoted as A. 128×640 $N=K=7$). The applied point loads (originally modelled as nodal forces in the shell model) were replaced by applied tractions that follow the exact distribution based on the first seven Fourier modes, in a manner consistent with the load characterization in the present solution (denoted as P. T. $N=K=7$). As expected, both solutions (P. T. $N=K=7$), and (A. 128×640 $N=K=7$) predict nearly identical displacements.

Locally, the Abaqus shell solution exhibits minor displacement fluctuations within the vicinity of the applied point load while the present solution predicts smoother displacement profiles. Two additional Abaqus models were developed based on the S8R shell element and the C3D20R brick element (both elements using quadratic interpolations as opposed to linear interpolation in the S4R element). For the C3D20R, two layers of elements were taken across the pipe thickness. Both models (not shown on Figure 12 to Figure 14 for clarity) were found to exhibit less fluctuation within the vicinity of the point load than the S4R model, i.e., their response is found closer to that of the present model.

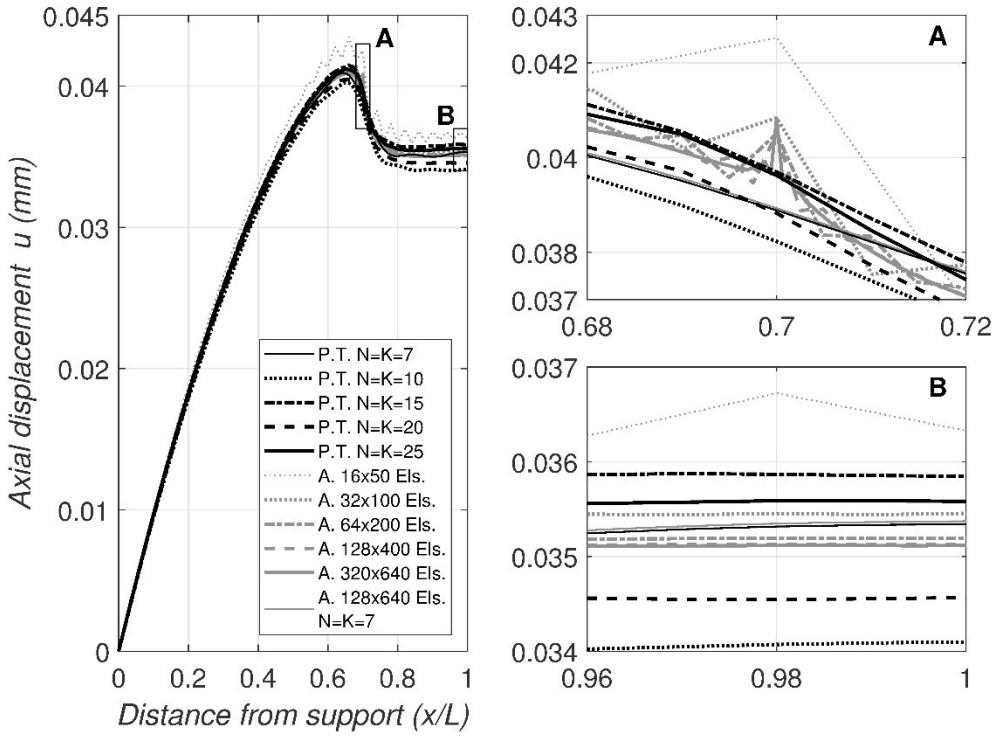

Figure 12 – Comparison of longitudinal displacements at top generator

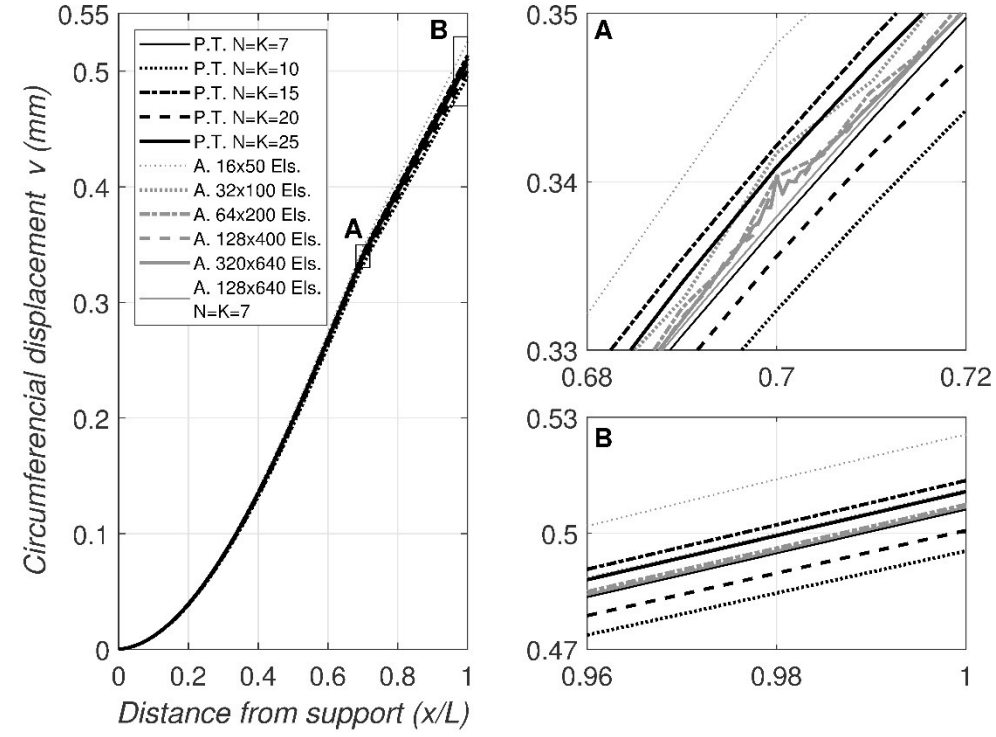

Figure 13 – Comparison of circumferential displacements at top generator

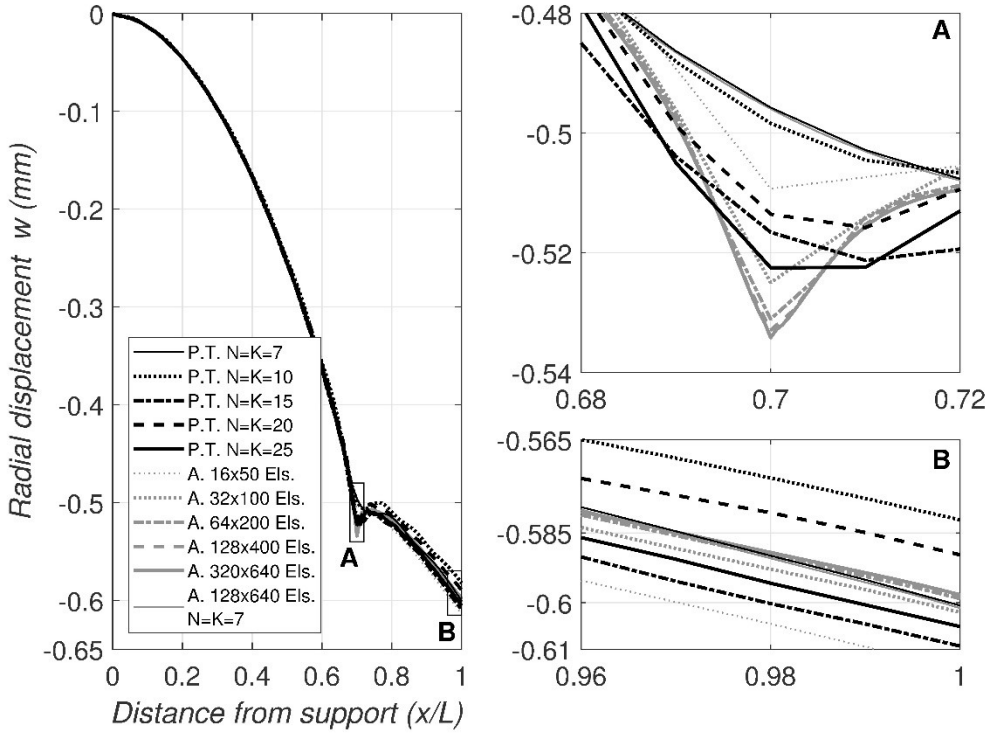

Figure 14 – Comparison of radial displacement at top generator

To investigate the effect of span on the results, three spans are considered; $L = 0.5\,m$, $L = 2.5\,m$ and $L = 5\,m$. The displacement components of the top generator ($s = z = 0$) versus the normalized longitudinal coordinate x / L are provided in Figure 15 to Figure 17. The number of modes taken is $N = K = 25$, which is beyond the number of modes required for convergence. Abaqus S4R meshes were based 240 elements in the circumferencial direction and 400 elements in longitudinal directions (a 240×400 mesh) for span $L = 0.5\,m$, a 128×200 mesh for span $L = 2.5\,m$, and a 128×640 mesh for span $L = 5\,m$).

As a general observation, all predictions are in very good agreement with the exception of the DMV theory. In addition, the difference between the responses predicted by the DMV solution and those of the other solutions tend to grow with the pipe span. In all cases, the DMV solution underestimates the dispacements compared to other solutions.

The maximum difference between the present solution results and those based on Abaqus are negligible. In general, the present theory predicts a slightly more flexible response compared to that of the Abaqus model with fine meshes. Irrespective of the span, the present theory's

predictions are in excellent agreement with Flugge's predictions, while the predictions of the Timoshenko's theory tend to deviate slightly from those of the two theories for shorter spans.

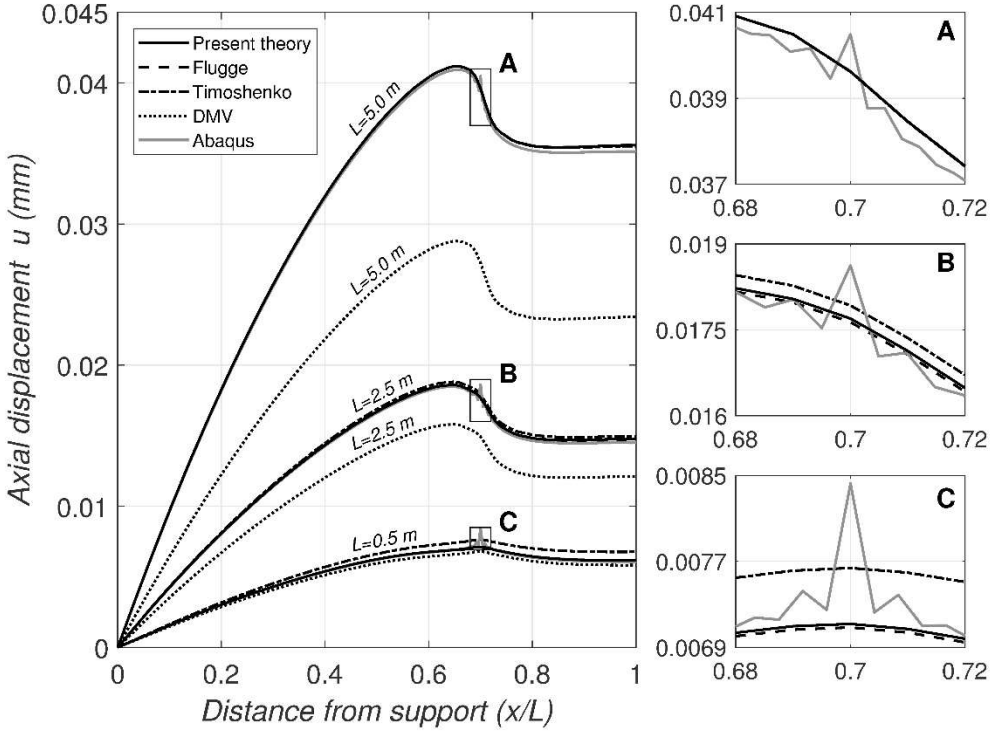

Figure 15 - Longitudinal displacement at the top generator

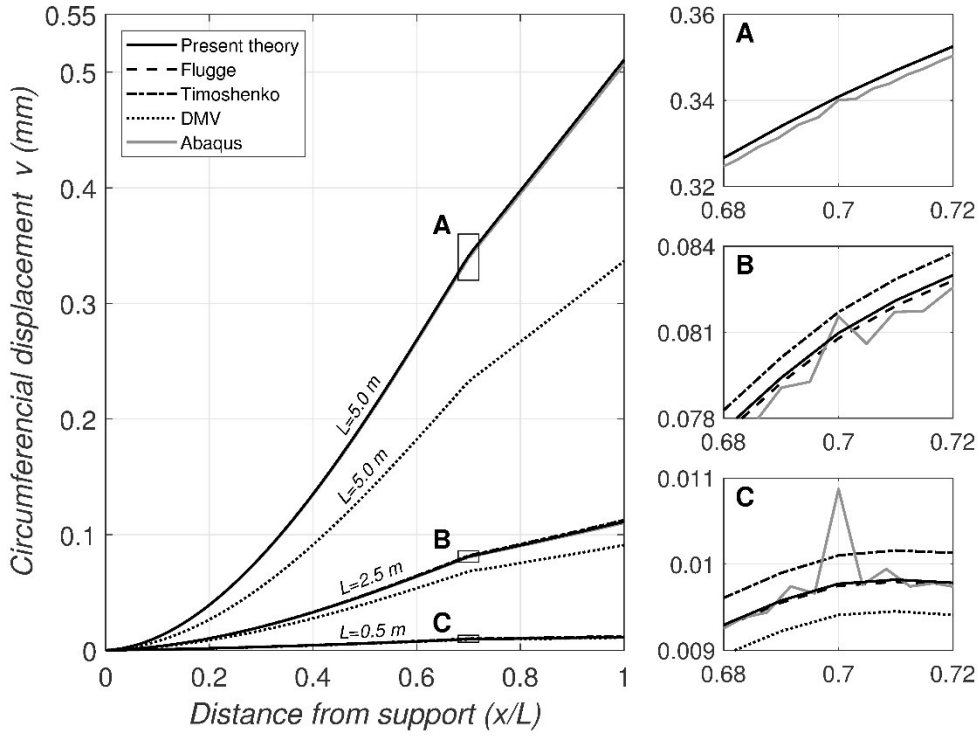

Figure 16 - Circumferential displacement at the top generator

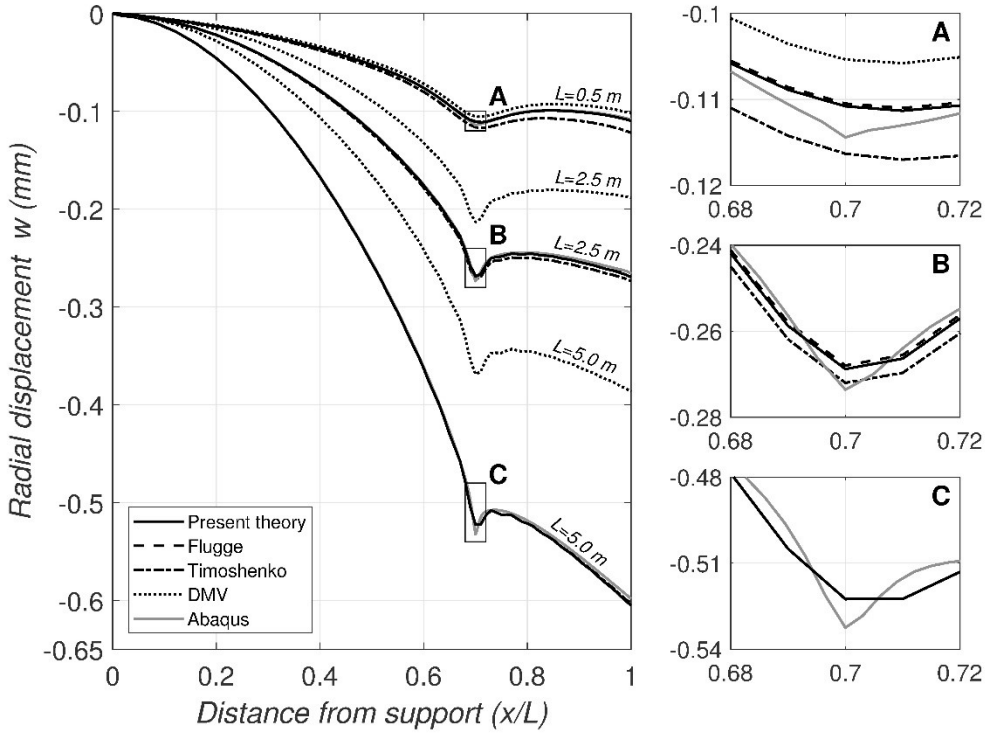

Figure 17 - Radial displacement at the top generator

To investigate the effect of thickness on various theories, the problem defined in the current example ($L = 5\,m$ and $R = 250\,mm$, with the same point load) is solved again while varying the thickness to $h = 5.0,\ 12.5,\ 25.0\ \ mm$, which correspond to radius to thickness values of $R/h = 50,\ 20,\ 10$, respectively). The problems are solved using two types of Abaqus models: one is based on 128×400 S4R Shell elements and the other is based on $4 \times 128 \times 400$ C3D8R Brick elements.

As shown in Figure 18 to Figure 20, predictions of the present theory, Flugge, and Timoshenko are in near perfect agreement, while Abaqus solutions provide an indistinguishable stiffer response. As the DMV results were far from the comparable range, they were not included in the plots. For the thicker pipe, the Timoshenko theory shows a negligibly more flexible response. In the proximity of the point load application, the finite element solutions exhibit localized oscillations, particularly for the brick element solution, which contrasts with the smoothness of the shell responses.

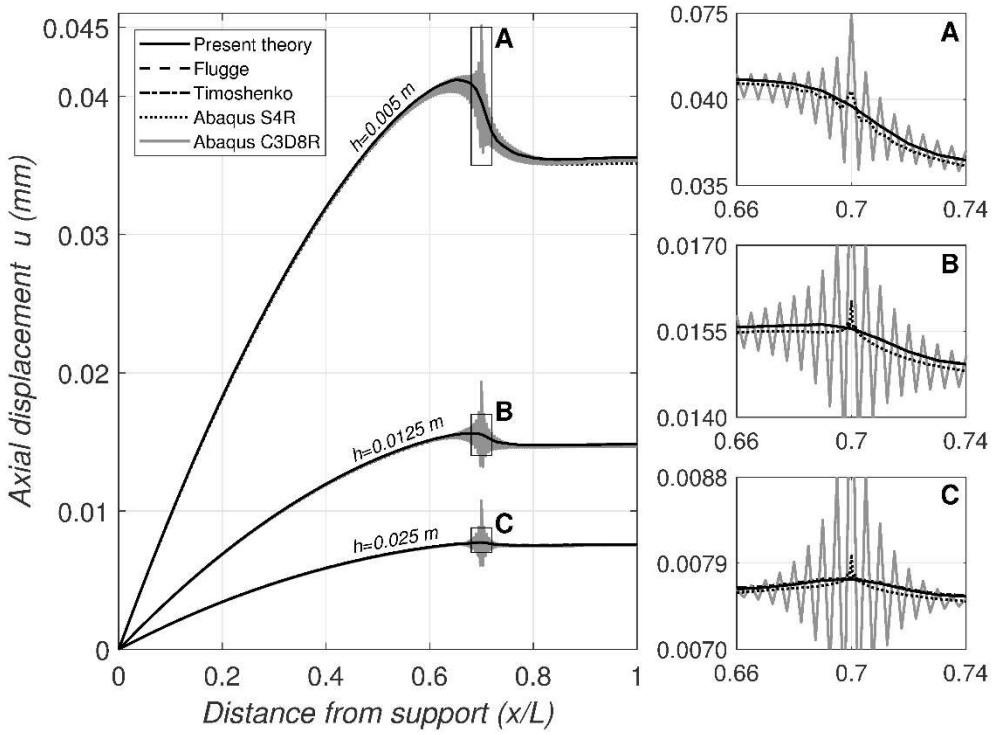

589

590 **Figure 18 - Longitudinal displacement on the top generator for various theories and different Abaqus**
591 **elements**

592

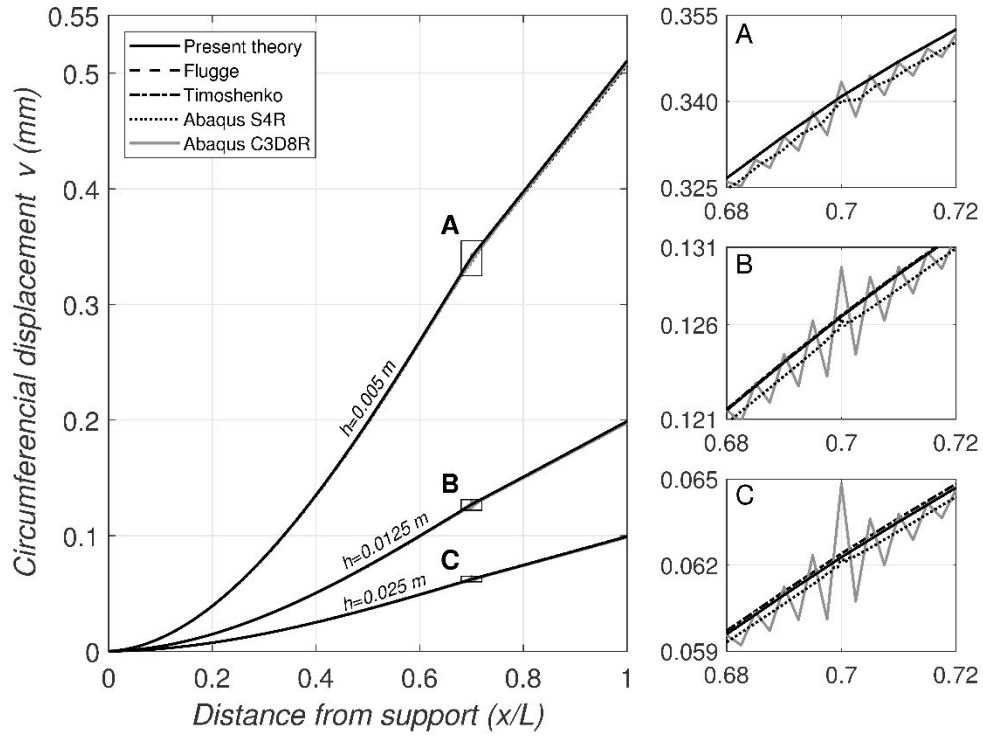

593

594 **Figure 19 - Circumferential displacement on the top generator for various theories and different Abaqus**
595 **elements**

596

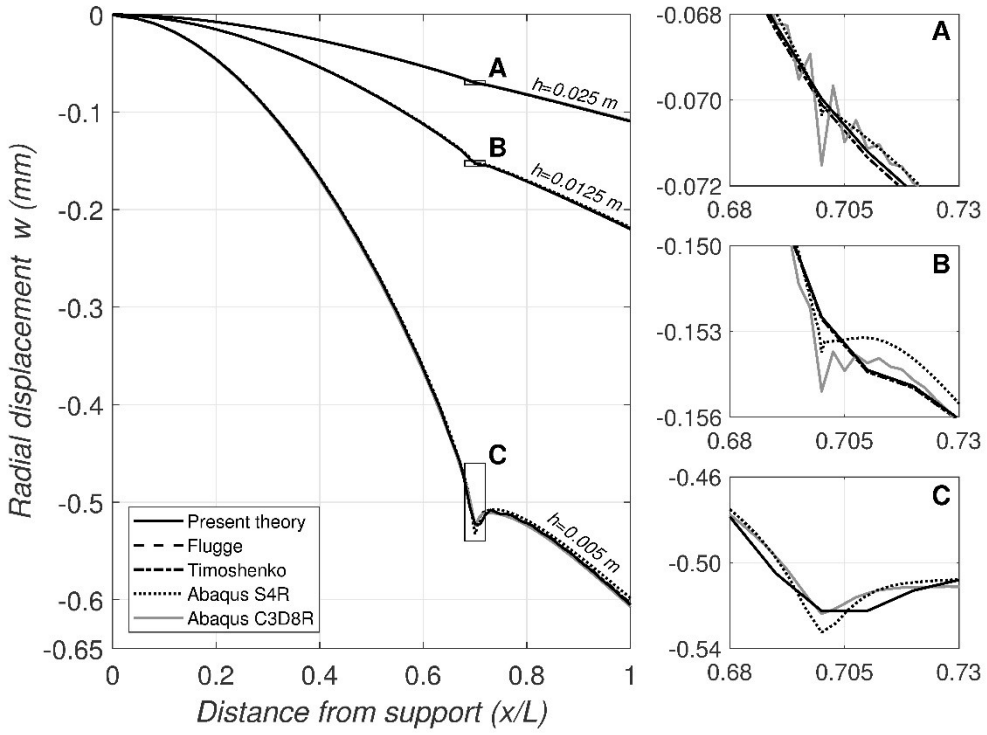

597

598 **Figure 20 - Radial displacement on the top generator for various theories and different Abaqus elements**

3.9.4 Example 4 – Comparisons against experimental results and analytical predictions

The natural frequencies based on the present theory are compared to the experimental results reported in [42]. The specimens tested were made of steel ($E = 200\,GPa$, $\rho = 7760\,kg/m^3$, $\nu = 0.29$) with span $L = 0.664\,m$, radius $R = 175\,mm$, thickness $h = 1.02\,mm$. Figure 21 depicts excellent agreement between the predictions of the present theory and the experimental results. Symbol n denotes the circumferential wave number and symbol ψ denotes the longitudinal half-wave number and satisfies the relation $m = \psi\pi i/L$. The present theory tends to predict slightly higher natural frequencies for higher circumferential modes. In all cases, the maximum difference between the present theory predictions and experimental results is 1.5%.

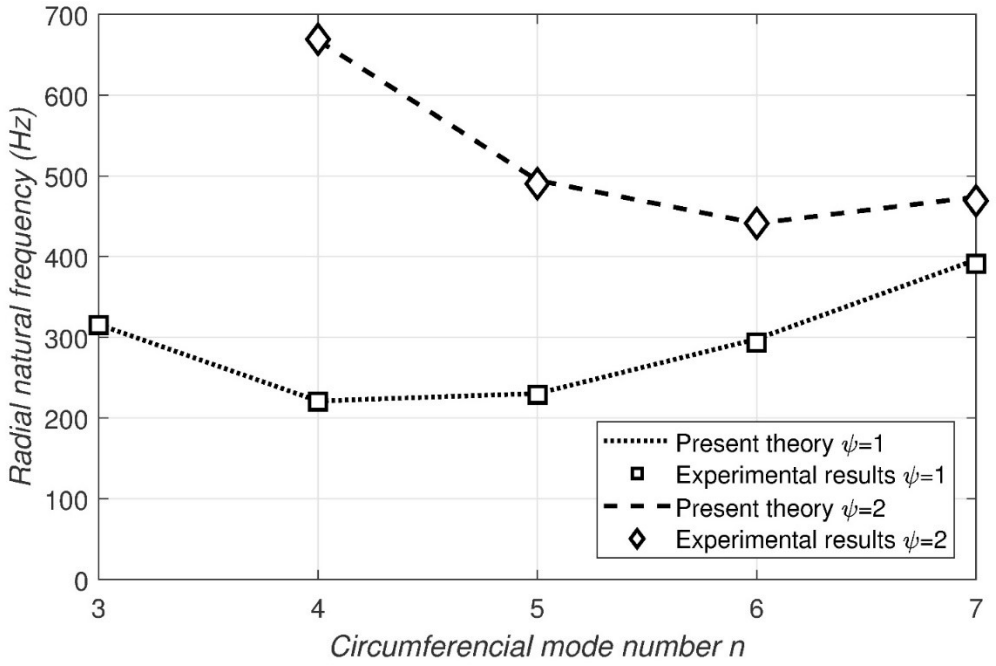

Figure 21 – Comparing natural frequencies

Additional comparisons are made against the analytical predictions in [43] which reported the natural frequencies for a simply supported pipe made of rubber ($E = 0.45\,GPa$, $\nu = 0.45$, $\rho = 1452\,kg/m^3$), span $L = 0.2\,m$, radius $R = 100\,mm$, and thickness $h = 2\,mm$. Table 5 shows that, for $\psi = 1,...,8$ and $n = 1,...,10$, the present theory is found to yield natural frequencies of up to 1.36% lower than the values reported in [43].

Table 5 – Comparing natural frequencies based on the present theory with analytical results

			ψ							
			1	2	3	4	5	6	7	8
n	1	Present	523.6	782.2	849.8	889.8	938.8	1011.8	1117.4	1260.3
		Ref. [43]	524.1	783.7	852.8	894.8	946.2	1021.9	1130.4	1276.5
		Diff. %	-0.09	-0.19	-0.35	-0.55	-0.78	-0.99	-1.15	-1.27
	2	Present	303.4	607.2	752.4	834.8	907.6	995.5	1111.2	1261.0
		Ref. [43]	303.9	609.1	755.8	840.1	915.3	1005.8	1124.3	1277.3
		Diff. %	-0.17	-0.32	-0.44	-0.64	-0.84	-1.02	-1.17	-1.28
	3	Present	188.1	456.1	641.2	763.7	865.6	973.9	1104.1	1264.0
		Ref. [43]	188.6	458.4	645.2	769.7	873.8	984.6	1117.4	1280.5
		Diff. %	-0.28	-0.50	-0.63	-0.78	-0.94	-1.08	-1.19	-1.28
	4	Present	149.5	355.8	546.7	695.7	823.9	953.6	1100.0	1272.0
		Ref. [43]	150.0	358.2	551.4	702.5	832.9	964.9	1113.8	1288.8
		Diff. %	-0.33	-0.66	-0.85	-0.97	-1.08	-1.17	-1.24	-1.30
	5	Present	167.3	309.9	485.4	645.6	792.9	941.4	1103.4	1287.6
		Ref. [43]	167.6	312.1	490.2	653.0	802.7	953.4	1117.9	1305.0
		Diff. %	-0.21	-0.69	-0.99	-1.13	-1.22	-1.26	-1.29	-1.33
	6	Present	218.4	314.5	463.9	622.9	780.9	943.2	1118.5	1313.7
		Ref. [43]	218.7	316.2	468.4	630.4	791.0	955.8	1133.6	1331.7
		Diff. %	-0.13	-0.53	-0.96	-1.18	-1.28	-1.32	-1.33	-1.35
	7	Present	288.7	358.4	481.9	631.7	792.5	963.3	1148.3	1352.5
		Ref. [43]	289.0	359.7	485.7	638.7	802.6	976.2	1163.9	1371.1
		Diff. %	-0.11	-0.36	-0.79	-1.10	-1.26	-1.32	-1.34	-1.36
	8	Present	372.9	429.2	533.1	670.9	829.4	1003.7	1194.8	1405.6
		Ref. [43]	373.3	430.4	536.3	677.2	839.0	1016.5	1210.7	1424.7
		Diff. %	-0.11	-0.27	-0.60	-0.93	-1.15	-1.26	-1.31	-1.34
	9	Present	469.4	519.1	610.0	736.9	890.3	1064.7	1258.9	1474.0
		Ref. [43]	470.0	520.2	612.8	742.5	899.3	1077.2	1274.8	1493.5
		Diff. %	-0.13	-0.22	-0.45	-0.76	-1.00	-1.16	-1.25	-1.31
	10	Present	577.6	623.9	706.9	825.2	972.9	1145.4	1340.5	1557.9
		Ref. [43]	578.5	625.2	709.6	830.3	981.4	1157.6	1356.4	1577.8
		Diff. %	-0.16	-0.21	-0.38	-0.62	-0.86	-1.05	-1.18	-1.26

4. Summary and Conclusions

A variational expression is developed for the dynamic analysis of thin shells of general geometries based on tensor calculus in conjunction with the Hamilton variational principle. The solution is based on a minimal number of assumptions at the outset of the formulation while avoiding non-essential approximations advocated in past theories. The variational expression is then specialized to CCTS and used to formulate the governing equilibrium equations and boundary conditions. The governing equations thus obtained are free from non-essential approximations and can potentially serve as a benchmark to assess the accuracy of

past circular cylindrical thin shell theories. The field equations derived are then compared to those of Flugge, Timoshenko, Novozhilov, Morley-Koiter, Niordson, Saada and DMV. A number of problems were numerically investigated using the present theory and comparisons were made with the Flugge, Timoshenko, and DMV theories.

The main conclusions of the study are:

(1) The governing field equations of the Flugge and DMV theories were recovered as special cases from the present theory by applying consistent approximations relating to the radius-to-thickness ratio to the governing equations derived herein.

(2) Compared to the present treatment, the theories of Timoshenko, Novozhilov, Morley-Koiter, Niordson, and Saada were found to involve inconsistent approximations. In some cases, such inconsistencies lead to over-simplifications in the field equations, while in others, they lead to the emergence of additional/unnecessary terms.

(3) The inconsistent simplifications made in the above theories do not necessarily correspond to a significant reduction in their predictive power. Specifically, the inconsistencies involved in Timoshenko's theory are of a small order and do not significantly influence its predictive ability. For DMV, while the approximations made are of a consistent order, the order of approximation implied happens to be too coarse to capture the response of pipes with moderate thicknesses.

(4) Numerical predictions of the 3D and shell FEA solutions are in excellent agreement with those of the present theory for a wide range of pipe dimensions ($2 < L/R < 20$ and $10 < R/h < 50$).

(5) The numerical predictions of the Flugge theory are found to be consistently in excellent agreement with those of the present theory and Abaqus finite element solutions, and is thus advocated as a more simplified CCTS theory, but yet as an accurate alternative to the present theory.

(6) In contrast, DMV exhibits an overly stiff behaviour compared to the present and other theories. In addition, it grossly overestimates the stresses in some cases. The theory is suitable only for very thin pipes.

Acknowledgement

The authors would like to express their deepest gratitude to the Baha´i Institute for Higher Education (BIHE), Tehran, Iran for its encouragement and support to the first author. Also, research funding from the Natural Science and Engineering Research Council of Canada (NSERC) to the second author is gratefully acknowledged.

5. List of Symbols

$\mathbf{a}_i$	Covariant base vectors of the middle surface
a_{ij}	First fundamental tensor defined on the middle surface of a thin shell
a	Determinant of the first fundamental tensor a_{ij}
$b_{\alpha\beta}$	Curvature tensor of the surfaces parallel and adjacent to the middle surface
$\overline{b}_{\alpha\beta}$	Second fundamental tensor or curvature tensor defined on the middle surface of a thin shell
$\mathbf{a}^i$	Contravariant base vectors of the middle surface
a^{ij}	First fundamental tensor of the second kind defined on the middle surface of a thin shell
$\mathbf{g}_i$	Covariant base vectors of any surface parallel and adjacent to the middle surface
g_{ij}	First fundamental tensor defined within the shell
g	Determinant of the first fundamental tensor g_{ij}
$\mathbf{g}^i$	Contravariant base vectors of any surface parallel and adjacent to the middle surface
g^{ij}	First fundamental tensor of the second kind defined within the shell
p^x, p^y, p^z	Physical components of the Contravariant body force components F^i as a function of (x,s,z,t)
$\overline{p}^x, \overline{p}^y, \overline{p}^z$	Physical components of the Contravariant body force components F^i as a function only of (x,s,z).
$\mathbf{R}$, $\mathbf{r}$	Position vector of a point within the shell and on the middle surface, respectively, before deformation.
$\hat{\mathbf{R}}$, $\hat{\mathbf{r}}$	Position vector of a point within the shell and on the middle surface, respectively, after deformation.
$\mathbf{U}$, $\mathbf{u}$	Displacement of a point within the shell and on the middle surface, respectively.
U_i , U^i	Covariant and contravariant components of the displacement of a point on a surface parallel and adjacent to the middle surface along axis x^i, respectively.
u_i	Covariant components of the displacement of a point on the middle surface along axis x^i
u, v, w	Components of the displacement of a point on the middle surface along axes x^1, x^2 and x^3, respectively
χ^i	Coordinate system/Coordinates of the system
x^i	Coordinate system/Coordinates of the system
x, s, z	Coordinates of the system, equivalent to x^1, x^2 and x^3 , respectively
$^{\alpha}, _{\alpha}, \ldots$	All Greek superscripts or subscripts range from 1 to 2
$^{i}, _{i}, \ldots$	All Italic superscripts or subscripts range from 1 to 3

$\vec{\mathbf{i}}_i, \vec{\mathbf{j}}_i$	Covariant unit vectors along axis x^i in middle surface and adjacent surfaces, respectively
$\vec{\mathbf{i}}^i, \vec{\mathbf{j}}^i$	Contravariant unit vectors along axis x^i in middle surface and adjacent surfaces, respectively
Γ_{ij}^k	Christoffel symbols in terms of g_i and g_{ij}
$\bar{\Gamma}_{ij}^k$	Christoffel symbols in terms of a_i and a_{ij} (defined for the middle surface)
$\cdot$	Inner product
$\otimes$	Cross product
$\vert$	Covariant derivative
$\Vert$	Covariant derivative in two dimensional spaces
T^*	Kinetic energy
V^*	Potential energy
V	Volume
W^*	External work
$\prod$	Mechanical energy of the system
ε_{ij}	Components of the strain tensor on the middle surface
η_{ij}	Components of the strain tensor on surfaces adjacent to the middle surface
$\eta_{\alpha\beta}$	In-plane components of the strain tensor
$\tilde{\eta}_{\alpha\beta}$	Physical components of $\eta_{\alpha\beta}$
σ^{ij}	Stress tensor
$\sigma^{\alpha\beta}$	In-plane components of the stress tensor σ^{ij}
ψ	Longitudinal half-wave number
E^{ijlm}	Generalized Hooke's Law
$E^{\alpha\beta\lambda\delta}$	In-plane components of the generalized Hooke's Law E^{ijlm}
$\cdots_{,i}$	Partial derivative with respect to x^i
δ_β^α	Kronecker delta function
μ_β^α	Mixed shifter tensor connecting the covariant base vectors of an arbitrary point within the shell to corresponding base vectors of the middle surface.
λ_α^γ	Inverse of mixed shifter tensor μ_β^α
ρ	Density of the mass
E	Modulus of elasticity
ν	Poisson's ratio
t	time

6. References

[1] S. Timoshenko, Theory of Plates and Shells. McGraw-Hill Book Company, New York, 1959.

[2] V.V. Novozhilov, Thin Shell Theory. P. Noordhoff Ltd. –Groningen-The Netherlands, 1964.

[3] W. T. Koiter, On the mathematical foundation of shell theory, Actes. Congres intern. Math. 3 (1970) 123-130.

[4] W. Flugge, Stresses in Shells. Springer-Verlag, New York Heidelberg Berlin, 1973.

[5] W. Flugge, Tensor Analysis and Continuum Mechanics, Springer-Verlag, New York Heidelberg Berlin, 1972.

[6] A. S. Saada, Elasticity: Theory and Applications, Pergamon Press Inc., New York, 1974.

[7] F. I. Niordson, Shell Theory. North-Holland Series In Applied Mathematics and Mechanics, 1985.

[8] R. W. Leonard, Nonlinear First Approximation Thin Shell and Membrane Theory. Ph. D. Dissertation, Virginia Polytechnic Institute, Blacksburg, Virginia, 1961.

[9] J. L. Sanders Jr., Nonlinear Theories for Thin Shells, Q. J. Appl. Math. 21 (1) (1963) 21-36.

[10] W. T. Koiter, On the Nonlinear Theory of Thin Elastic Shells. Proceedings of the Koninklijke Nederlandse Akademie van Wetenschappen, Series B, 69 (1966) 1-54.

[11] W. T. Koiter, General Equations of Elastic Stability for Thin Shells. Proceedings-Symposium on the Theory of Shells, University of Houston, (1967), 187-227.

[12] B. Budiansky, Notes on Nonlinear Shell Theory, J. Appl. Mech. 35 (2) (1968) 393-401.

[13] A.W. Leissa, Vibration of Shells, Acoust. Soc. Am., 1993.

[14] A. Libai, C. W. Bert, A mixed variational principle and its application to the nonlinear bending problem of orthotropic tubes-I. Development of general theory and reduction to cylindrical shells, Int. J. Solids Struct. 31 (7) (1994) 1003-1018.

[15] A. -H. Muneeb, G. A. Birlik, Y. Mengi, A higher order dynamic theory for isotropic thermoelastic cylindrical shells: Part 1: Theory, J. Sound Vib. 179 (5) (1995) 817-826.

[16] S. V. Kolesnikov, A refined theory of the vibrations of a cylindrical shell based on an expansion in series of the normal displacement, J. Appl. Math. Mech. 60 (1) (1996) 113-119.

694 [17] F. I. Niordson, An asymptotic theory for circular cylindrical shells, Int. J. Solids Struct.
695 37 (13) (2000) 1817-1839.
696 [18] S. V. Ugrimov, Generalized theory of multilayer plates, Int. J. Solids Struct. 39 (4) (2002)
697 819-839.
698 [19] P. G. Ciarlet, L. Gratie, Another approach to linear shell theory and a new proof of Korn's
699 inequality on a surface, Mathematical Problems in Mechanics, C. R. Acad. Sci. Paris, Ser.
700 I 340 (2005).
701 [20] M. Birsan, On the theory of elastic shells made from a material with voids, Int. J. Solids
702 Struct. 43 (2006) 3106-3123.
703 [21] H. Altenbach, V. A. Eremeyev, N. F. Morozov, Linear theory of shells taking into account
704 surface stresses. Dokl. Phys. 54 (12) (2009) 531-535.
705 [22] K. Weicker, R. Salahifar, M. Mohareb, Shell analysis of thin-walled pipes. Part I - Field
706 equations and solution, Int. J. Press. Vessels Pip. 87 (7) (2010) 402-413.
707 [23] K. Weicker, R. Salahifar, M. Mohareb, Shell analysis of thin-walled pipes. Part II - Finite
708 element formulation, Int. J. Press. Vessels Pip. 87 (7) (2010) 414-423.
709 [24] R. Salahifar, M. Mohareb, Analysis of circular cylindrical shells under harmonic forces,
710 Thin Walled Struct. 48 (7) (2010) 528-539.
711 [25] M. Amabili, J. N. Reddy, A new non-linear higher-order shear deformation theory for
712 large-amplitude vibrations of laminated doubly curved shells, Int. J. Non Linear Mech.
713 45 (4) (2010) 409-418.
714 [26] V. N. Paimushin, A theory of thin shells with finite displacements and deformations based
715 on a modified Kirchhoff-Love model, J. Appl. Math. Mech. 75 (5) (2011) 568-579.
716 [27] R. Salahifar, M. Mohareb, Finite element for cylindrical thin shells under harmonic
717 forces, Finite Elem. Anal. Des. 52 (2012) 83-92.
718 [28] A. Favata, P. Podio-Guidugli, A new CNT-oriented shell theory, Eur. J. Mech. A. Solids
719 35 (2012) 75-96.
720 [29] C. Sansour, S. Skatulla, M. Hjiaj, A shell theory with scale effects and higher order
721 gradients, Int. J. Solids Struct. 50 (2013) 2271-2280.
722 [30] J. Xuea, D. Yuana, F. Hanb, R. Liua, An extension of Karman–Donnell's theory for non-
723 shallow, long cylindrical shells undergoing large deflection, Eur. J. Mech. A. Solids 37
724 (2013) 329-335.
725 [31] V. V. Zozulya, A high-order theory for functionally graded axially symmetric cylindrical
726 shells, Arch. Appl. Mech. 83 (3) (2013) 331-343.

[32] E Carrera, S. Brischetto, P. Nali, Plates and shells for smart structures: classical and advanced theories for modeling and analysis. John Wiley & Sons, 2011.
[33] E. Carrera, M. Cinefra, M. Petrolo, E. Zappino, Finite element analysis of structures through unified formulation. John Wiley & Sons, 2014.
[34] A. Cattabiani, H. Riou, A. Barbarulo, P. Ladevèze, B. Troclet, The Variational Theory of Complex Rays applied to the shallow shell theory, Comput. Struct. 158 (2015) 98-107.
[35] S. R. Chowdhurya, P. Roya, D. Roya, J. N. Reddy, A peridynamic theory for linear elastic shells, Int. J. Solids Struct. 84 (2016) 110-132.
[36] Ye. M. Zveryayev, A consistent theory of thin elastic shells, J. Appl. Math. Mech. 80 (2016) 409-420.
[37] J. Awrejcewicz, V. A. Krysko, A. A. Sopenko, M. V. Zhigalov, A. V. Kirichenko, A. V. Kryskoc, Mathematical modelling of physically/geometrically non-linear micro-shells with account of coupling of temperature and deformation fields, Chaos, Solitons Fractals 104 (2017) 635-654.
[38] Q. Wangab, D. Shaoc, B. Qind, A simple first-order shear deformation shell theory for vibration analysis of composite laminated open cylindrical shells with general boundary conditions, Compos. Struct. 184 (15) (2018) 211-232.
[39] R. Okhovat, A. Bostrom, Dynamic equations for an orthotropic cylindrical shell, Compos. Struct. 184 (2018) 1197-1203.
[40] Q. Wang, D. Shao, B. Qin, A simple first-order shear deformation shell theory for vibration analysis of composite laminated open cylindrical shells with general boundary conditions, Compos. Struct. 184 (2018) 211-232.
[41] R. Salahifar, Analysis of Pipeline Systems under Harmonic Forces, Ph. D. Thesis, Department of Civil Engineering, University of Ottawa, Ontario, Canada, 2011.
[42] M. Amabili, G. Dalpiaz, Breathing vibrations of a horizontal circular cylindrical tank shell, partially filled with liquid, J. Vib. Acoust. 117 (1995) 187-191.
[43] I. Senjanović, I. Ćatipović, N. Alujević, N. Vladimir, D. Čakmak, A finite strip for the vibration analysis of rotating circular cylindrical shells, Thin Walled Struct. 122 (2018) 158-172.

Appendix A- Coefficients appearing in Hamilton functional for CCTS

$${}^{1}_{1}\bar{H} = -1 \quad , \quad {}^{1}_{2}\bar{H} = -\nu \quad , \quad {}^{1}_{3}\bar{H} = -\nu/R \quad , \quad {}^{1}_{4}\bar{H} = h^2/12R$$

$${}^{2}_{1}\bar{H} = -(1-\nu)/2 \quad , \quad {}^{2}_{2}\bar{H} = -(1-\nu)\left(1+h^2/4R^2\right)/2 \quad , \quad {}^{2}_{3}\bar{H} = (1-\nu)h^2/8R$$

$${}^{3}_{1}\bar{H} = -h^2/12R \quad , \quad {}^{3}_{2}\bar{H} = (1-\nu)R(\Phi-1)/2 \quad , \quad {}^{3}_{3}\bar{H} = -(3-\nu)h^2/24R$$

$${}^{3}_{4}\bar{H} = h^2/12 \quad , \quad {}^{3}_{5}\bar{H} = \left[(3-\nu)h^2/24 + (1-\nu)R^2(\Phi-1)/2\right]$$

$${}^{3}_{6}\bar{H} = \rho\left(1-\nu^2\right)h^2/12R\,E \quad , \quad {}^{3}_{7}\bar{H} = -\rho\left(1-\nu^2\right)h^2/12\,E$$

$${}^{3}_{8}\bar{H} = \left(1-\nu^2\right)/Eh$$

$${}^{4}_{1}\bar{H} = h^2/12R \quad , \quad {}^{4}_{2}\bar{H} = \nu h^2/12R \quad , \quad {}^{4}_{3}\bar{H} = -h^2/12$$

$${}^{4}_{4}\bar{H} = -\nu h^2/12$$

$${}^{1}_{1}\bar{G} = 1 \quad , \quad {}^{1}_{2}\bar{G} = (1-\nu)\Phi/2 \quad , \quad {}^{1}_{3}\bar{G} = (1+\nu)/2$$

$${}^{1}_{4}\bar{G} = \nu/R \quad , \quad {}^{1}_{5}\bar{G} = -h^2/12R$$

$${}^{1}_{6}\bar{G} = (1-\nu)R(\Phi-1)/2 \quad , \quad {}^{1}_{7}\bar{G} = -\rho\left(1-\nu^2\right)/E \quad ,$$

$${}^{1}_{8}\bar{G} = \rho\left(1-\nu^2\right)h^2/12RE \quad , \quad {}^{1}_{9}\bar{G} = \left(1-\nu^2\right)/Eh$$

$${}^{2}_{1}\bar{G} = (1+\nu)/2 \quad , \quad {}^{2}_{2}\bar{G} = (1-\nu)\left(1+h^2/4R^2\right)/2 \quad , \quad {}^{2}_{3}\bar{G} = 1$$

$${}^{2}_{4}\bar{G} = 1/R \quad , \quad {}^{2}_{5}\bar{G} = -(3-\nu)h^2/24R \quad , \quad {}^{2}_{a}\bar{G} = 0$$

$${}^{2}_{6}\bar{G} = -\rho\left(1-\nu^2\right)\left(1+h^2/12R^2\right)/E \quad , \quad {}^{2}_{7}\bar{G} = \rho\left(1-\nu^2\right)h^2/6RE \quad ,$$

$${}^{2}_{8}\bar{G} = \left(1-\nu^2\right)/Eh$$

$${}^{3}_{1}\bar{G} = -\nu/R \quad , \quad {}^{3}_{2}\bar{G} = -1/R \quad , \quad {}^{3}_{3}\bar{G} = -\Phi/R^2$$

$${}^{3}_{4}\bar{G} = -2(\Phi-1) \quad , \quad {}^{3}_{5}\bar{G} = h^2/12R$$

$${}^{3}_{6}\bar{G} = -(1-\nu)R(\Phi-1)/2 \quad , \quad {}^{3}_{7}\bar{G} = (3-\nu)h^2/24R \quad , \quad {}^{3}_{b}\bar{G} = 0$$

$${}^{3}_{8}\bar{G} = -h^2/12 \quad , \quad {}^{3}_{9}\bar{G} = -\left[(3+\nu)h^2/24 + (1-\nu)R^2(\Phi-1)/2\right]$$

$${}^{3}_{10}\bar{G} = -R^2(\Phi-1) \quad , \quad {}^{3}_{11}\bar{G} = -\rho\left(1-\nu^2\right)/E$$

$${}^{3}_{12}\bar{G} = \rho\left(1-\nu^2\right)h^2/12E \quad , \quad {}^{3}_{13}\bar{G} = \rho\left(1-\nu^2\right)h^2/12E$$

$${}^{3}_{14}\bar{G} = -\rho\left(1-\nu^2\right)h^2/12RE \quad , \quad {}^{3}_{15}\bar{G} = -\rho\left(1-\nu^2\right)h^2/6RE$$

757 $${}^{3}_{16}\bar{G} = -\left(1-\nu^2\right)/Eh \quad , \quad {}^{3}_{17}\bar{G} = -\left(1-\nu^2\right)/Eh$$

$${}^{3}_{18}\bar{G} = \left(1-\nu^2\right)/Eh$$

758 where $\Phi = \Phi(h/R) = (R/h)\ln\left[(2+h/R)/(2-h/R)\right]$

Appendix B - Force terms, Boundary Conditions and Field Equations

The terms $f^{xu}, f^{xw}, f^{sv}, f^{sw}, f^{zw}$ are related to the physical force components p^x, p^s, p^z per unit volume (of the contravariant external force components F^i, respectively) through the integrals

$$\begin{Bmatrix} f^{xu} \\ f^{sv} \\ f^{zw} \\ f^{xw} \\ f^{sw} \end{Bmatrix} = \int_{-\frac{h}{2}}^{+\frac{h}{2}} \begin{Bmatrix} p^x\left(1+z/R\right) \\ p^s\left(1+z/R\right)^2 \\ p^z\left(1+z/R\right) \\ p^x z\left(1+z/R\right) \\ p^s z\left(1+z/R\right) \end{Bmatrix} dz \tag{B.1a-e}$$

In Eq. 25, since t_1 and t_2 are arbitrary times and the variations δu, δv, δw and $\delta w_{,1}$ are arbitrary within the domain ($0 < x < L$ and $0 < s < 2\pi R$) , the first and second integrals have to vanish independently. The former integral yields eight boundary conditions,

$$\begin{aligned}
&\left[\left({}^1_1\bar{H}u_{,1} + {}^1_2\bar{H}v_{,2} + {}^1_3\bar{H}w + {}^1_4\bar{H}w_{,11}\right)\delta u\right]_0^L = 0 \\
&\left[\left({}^2_1\bar{H}u_{,2} + {}^2_2\bar{H}v_{,1} + {}^2_3\bar{H}w_{,12}\right)\delta v\right]_0^L = 0 \\
&\left[\left({}^3_1\bar{H}u_{,11} + {}^3_2\bar{H}u_{,22} + {}^3_3\bar{H}v_{,12} + {}^3_4\bar{H}w_{,111} + {}^3_5\bar{H}w_{,122} + {}^3_6\bar{H}\ddot{u} + {}^3_7\bar{H}\ddot{w}_{,1} + {}^3_8\bar{H}f^{xw}\right)\delta w\right]_0^L = 0 \\
&\left[\left({}^4_1\bar{H}u_{,1} + {}^4_2\bar{H}v_{,2} + {}^4_3\bar{H}w_{,11} + {}^4_4\bar{H}w_{,22}\right)\delta w_{,1}\right]_0^L = 0
\end{aligned} \tag{B.2}$$

in which either the bracketed expressions vanish, yielding the natural boundary conditions, or their respective coefficient does, yielding the essential boundary conditions, and the second integral of Eq. 25 yields the following three equilibrium equations.

$$\begin{aligned}
&\left({}^1_1\bar{G}u_{,11} + {}^1_2\bar{G}u_{,22} + {}^1_3\bar{G}v_{,12} + {}^1_4\bar{G}w_{,1} + {}^1_5\bar{G}w_{,111} + {}^1_6\bar{G}w_{,122} + {}^1_7\bar{G}\ddot{u} + {}^1_8\bar{G}\ddot{w}_{,1} + {}^1_9\bar{G}f^{xu}\right) = 0 \\
&\left({}^2_1\bar{G}u_{,12} + {}^2_2\bar{G}v_{,11} + {}^2_3\bar{G}v_{,22} + {}^2_4\bar{G}w_{,2} + {}^2_5\bar{G}w_{,112} + {}^2_a\bar{G}w_{,222} + {}^2_6\bar{G}\ddot{v} + {}^2_7\bar{G}\ddot{w}_{,2} + {}^2_8\bar{G}f^{sv}\right) = 0 \\
&\left({}^3_1\bar{G}u_{,1} + {}^3_2\bar{G}v_{,2} + {}^3_3\bar{G}w + {}^3_a\bar{G}w_{,11} + {}^3_4\bar{G}w_{,22} + {}^3_5\bar{G}u_{,111} + {}^3_6\bar{G}u_{,122} + {}^3_7\bar{G}v_{,112} + {}^3_b\bar{G}w_{,222}\right. \\
&\quad + {}^3_8\bar{G}w_{,1111} + {}^3_9\bar{G}w_{,1122} + {}^3_{10}\bar{G}w_{,2222} + {}^3_{11}\bar{G}\ddot{w} + {}^3_{12}\bar{G}\ddot{w}_{,11} + {}^3_{13}\bar{G}\ddot{w}_{,22} + {}^3_{14}\bar{G}\ddot{u}_{,1} + {}^3_{15}\bar{G}\ddot{v}_{,2} \\
&\quad \left. + {}^3_{16}\bar{G}f^{xw}_{,1} + {}^3_{17}\bar{G}f^{sw}_{,2} + {}^3_{18}\bar{G}f^{zw}\right) = 0
\end{aligned} \tag{B.3}$$